Environmental Science Advances

ROYAL SOCIETY OF CHEMISTRY

PAPER

View Article Online
View Journal | View Issue



Cite this: *Environ. Sci.: Adv.*, 2025, **4**, 676

# Geochemical speciation, pollution assessment, and source identification of heavy metals in sediment cores of the Cau River basin, Hai Duong province, Vietnam†

Ba Lich Pham, ‡*[a] Huy Thong Vu,[ab] Van Linh Nguyen,[a] Thi Kim Thuong Nguyen,[a] Anh Duc Trinh[c] and Thi Thao Ta*[a]

Heavy metal contamination in sediment has caused severe threats to the aquatic ecosystem and public health worldwide. Networks of rivers and their tributaries serve as dynamic habitats for these potentially harmful metals through aqueous–sedimentary equilibrium shifts. Hence, determining the distinct chemical forms of a given heavy metal in sediment is crucial for evaluating its bio-lability and toxicity. This study demonstrates the geochemical speciation using a sequential extraction procedure to fractionate individual phases (exchangeable, carbonate, Fe–Mn oxide, organic, and residual) of nine heavy metals (Cu, Pb, Cd, Zn, Fe, Co, Ni, Mn, and Cr) in the sediment of a river system in Hai Duong, a deltaic province in Vietnam. A quantitative assessment of environmental risk factors (*e.g.*, contamination factor and risk assessment code) and the pseudo-partitioning coefficient between pore water and sediment was conducted to define the pollution levels of heavy metals and their contaminated areas. Furthermore, multivariate analyses facilitate a profound comprehension of the contributions to pollution. Analyses of the extracts from the sequential extraction procedure were performed by inductively coupled plasma-mass spectrometry. The results of sedimentary heavy metal speciation indicate that the critical risks of Cd (15.8–38.4%) and Mn (16.3–53.8%) to the aquatic ecosystem are due to their higher retrieval from the exchangeable fraction. Additionally, an appreciable percentage of Co (26.3–58.0%), Mn (16.8–66.3%), Ni (16.0–53.1%), Pb (6.75–69.7%), and Zn (4.42–45.8%) in the carbonate fraction highlights a strong tendency for co-precipitation or ion exchange of these metals with carbonate minerals. Whilst colloids of Fe–Mn oxides act as efficient scavengers for metals such as Fe, Mn, Zn, and Pb, organic matter forms primarily function in trapping Cu, Pb, Fe, Cr, Co, and Ni. Our findings in the ecological risk evaluations and multivariate analyses indicate that Cr, Ni, and Fe are ascribed to natural lithogenic provenances. In contrast, anthropogenic inputs induce Cd, Mn, Cu, and Pb high-environmental risks.

Received 25th August 2024
Accepted 14th February 2025

DOI: 10.1039/d4va00325j

rsc.li/esadvances



## Environmental significance

Heavy metals are critically hazardous pollutants that pose a significant threat to public health due to their accumulation in the food chain. Deciphering their transport mechanisms between the water phase and sediment in river systems is crucial not only for tracing their emission sources but also for devising remediation strategies and sustainable development measures to protect aquatic ecosystems. This study conducted a comprehensive and methodical investigation of their pollution levels in a municipal watercourse system in Hai Duong, part of Vietnam's Northern Key Economic Zone. The findings indicate that high-risk elements predominantly liberate from urban runoff, sewage drainage, and industrial wastewater discharge, while low-risk metals are primarily ascribed to lithogenic origins. These observations will provide valuable references for local authorities to implement prompt supervision and solutions for managing toxic metals on the surface waters of Hai Duong province.

[a]*Department of Analytical Chemistry, Faculty of Chemistry, VNU University of Science, 19 Le Thanh Tong Street, Hanoi 100000, Vietnam. E-mail: phambalichls@gmail.com; tathithao@hus.edu.vn*

[b]*Fundamental Sciences Department, University of Fire Fighting and Prevention, Hanoi 100000, Vietnam*

[c]*Nuclear Training Center, Vietnam Atomic Energy Institute, 140 Nguyen Tuan, Thanh Xuan, Hanoi 100000, Vietnam*

† Electronic supplementary information (ESI) available. See DOI: https://doi.org/10.1039/d4va00325j

‡ Present address: Institut de Chimie Physique, Université Paris-Saclay, Centre National de la Recherche Scientifique (CNRS), UMR8000, 91405 Orsay, France.

## 1. Introduction

Nowadays, the pollution of heavy metals (HMs) in the aquatic environment is a global concern due to their potent effects on the food chain, particularly humans. HMs are naturally found on Earth but in stable and benign forms. However, anthropogenic activities tend to accumulate them in bio-available forms.[1] The increase of HMs in labile forms is attributed to natural sources and anthropogenic activities such as industrial

development, mining and refining, agricultural drainage, domestic discharges, and atmospheric deposition.[2] Consequently, their genotoxicity and carcinogenicity, persistence, and abiotic degradation in the ecological system pose a serious risk to human health. Specifically, the respiratory, nervous, reproductive, and digestive systems are particularly susceptible to HMs and may even display apoptosis/necrosis pathways.[3,4]

HMs transported into aquatic systems are mainly incorporated into sediments through adsorption, flocculation, ion exchange, precipitation, and complexation in the water column.[5,6] Sediments serve as the archive of HMs and therefore become the storage of potentially hazardous metals.[7] HMs entering natural water become part of the water column–sediment system, and their distribution is controlled by a dynamic equilibrium of numerous physico-chemical processes. HM dissolution occurs as a function of environmental conditions (*e.g.*, temperature, pH, redox potential, electrical conductivity, and organic ligand contents), which usually increase contamination of aquatic systems.[8] The potential for environmental pollution can be diminished if these metals are locked in sediments.[9] However, HMs are not permanently trapped in sediment due to exchange processes of metals with carbonates, oxides, sulfides, organometallic compounds, and ions in the crystal lattice of minerals such as Fe(III) stored in ferrihydrite. Providing only data on the metal abundance in samples, total HM concentrations could not be the basis for assessing the toxicity and potential risks of metal pollutants.[10,11] Different forms of a given metal have different impacts on the ecosystem. Therefore, it is necessary to conduct metal speciation analysis in sediments to estimate the actual impacts and the mobility of metals *via* downstream transport, deposition, and release to biota under environmental condition changes.[12] Various studies have recently investigated and reported contaminated conditions with distinctive spatial and temporal distributions and ecotoxicological impacts of HMs in sediments along rivers/lakes across different regions, *e.g.*, Brazil,[13] Greece,[14] Turkey,[1] Bangladesh,[15] India,[16,17] Pakistan,[18–21] Egypt,[22,23] Iran,[24–26] China,[27–34] *etc.*

Speciation refers to a description of the chemical forms of metal–ligand complexes in the aqueous phase. In the study of geochemical speciation in sediment, the total content of metals is partitioned into five different specific fractions, distinguishing binding phases in the descending order of mobility. Sinks for water-soluble or exchangeable metals fall into the phase 1 category ($F_1$). Geochemical phase 2 presents the tendency to precipitate in the lattice of secondary minerals like carbonates, sulfides, phosphates, or oxides (weakly absorbed-$F_2$). Metals occluded in amorphous materials such as Fe–Mn oxy-hydroxide are classified into phase 3 (reducible-$F_3$). Lastly, metals complexed with organic matter (humin, humic and fulvic acids containing various functional groups: hydroxyl –OH, carbonyl C=O, carboxyl –COOH) (oxidizable-$F_4$) or chemisorbed on the lattice of primary and secondary minerals such as silicates (residual-$F_5$) respectively constitute the final two categories.[35,36] Amongst different methods to elucidate the so-called "solid/particulate speciation", sequential extraction procedures (SEPs) were developed to more accurately separate labile fractions (inorganic and organic) from residual phases and to help quantify the biolability of different pollutants and trace HMs associated with soils and sediments.[37] Sequential extraction techniques are able to provide the origin of metal input, digenetic transformation within the sediments, and the reactivity of HM species of both natural and anthropogenic attribution.[12]

Depending upon the required sensitivity, versatility, sample matrix, and applications, various analytical techniques are available for analyzing trace levels of HMs. These include graphite furnace atomic absorption spectroscopy (GFAAS),[38] cold vapor atomic absorption spectroscopy (CV-AAS),[39,40] X-ray fluorescence (XRF) spectroscopy,[41–43] anodic stripping voltammetry (ASV),[44,45] inductively coupled plasma optical emission spectroscopy (ICP-OES),[46,47] inductively coupled plasma-mass spectrometry (ICP-MS),[15,48] and high-performance liquid chromatography (HPLC) coupled with inductively coupled plasma-mass spectrometry (ICP-MS).[49,50] Nevertheless, specialized techniques are particularly suited for different capabilities, such as XRF and ICP-OES for trace detection (ppm–ppb levels). Some are effective for ultra-trace (ppt) single-element analysis such as GFAAS and CV-AAS, which is specific and sensitive for mercury (Hg) only (ppm, ppb, and ppt signify parts per million, parts per billion, and parts per trillion, respectively). Techniques like ASV, ICP-OES, and XRF require expertise to address matrix interference in complex samples. Amongst these, ICP-MS is considered the gold standard due to its unparalleled sensitivity and versatility, making it an ideal and well-suited choice for simultaneous multi-element analysis at ultra-trace levels. The coupling of HPLC with ICP-MS is excellent for speciation in complex matrices (*e.g.*, organic and inorganic arsenic species[50]) but entails intricate and advanced instrumentation and is relatively more time-consuming compared to direct methods. Thus, employing SEP alongside ICP-MS for trace metal speciation in sediment provides valuable insights into the chemical forms and potential deficiencies of HMs in sediment.

Hai Duong is a northeastern province located in the Northern Key Economic Zone (NKEZ) that has experienced rapid industrial and urban development in Vietnam (Fig. 1). Specifically, Hai Duong has a large population (2.567 million in 2019) and a number of industrial zones such as Lai Vu, Nam Sach, Tan Truong, Trang Due, *etc.* In addition, due to the intensive agriculture in Hai Duong, there are numerous local waterways for irrigation and drainage. According to the Vietnamese Department of Natural Resources and Environment (DNRE), Hai Duong has recently been impacted significantly by pollution from industrial zones.[51,52] Therefore, wastewater and pollutants are mainly released into sewage and river systems. There are a few publications about pollution circumstances in Hai Duong that assessed the quality of surface water and the nutrient pollution source using multivariate statistical techniques[53] and interpreted the anthropogenic impacts through the spatio-temporal variation of stable isotopes of $NO_3^-$.[54] In these previous studies, it was mentioned that the pollution in the Hai Duong river systems resulted primarily from an accumulation of anthropogenic pollution. However, none of these

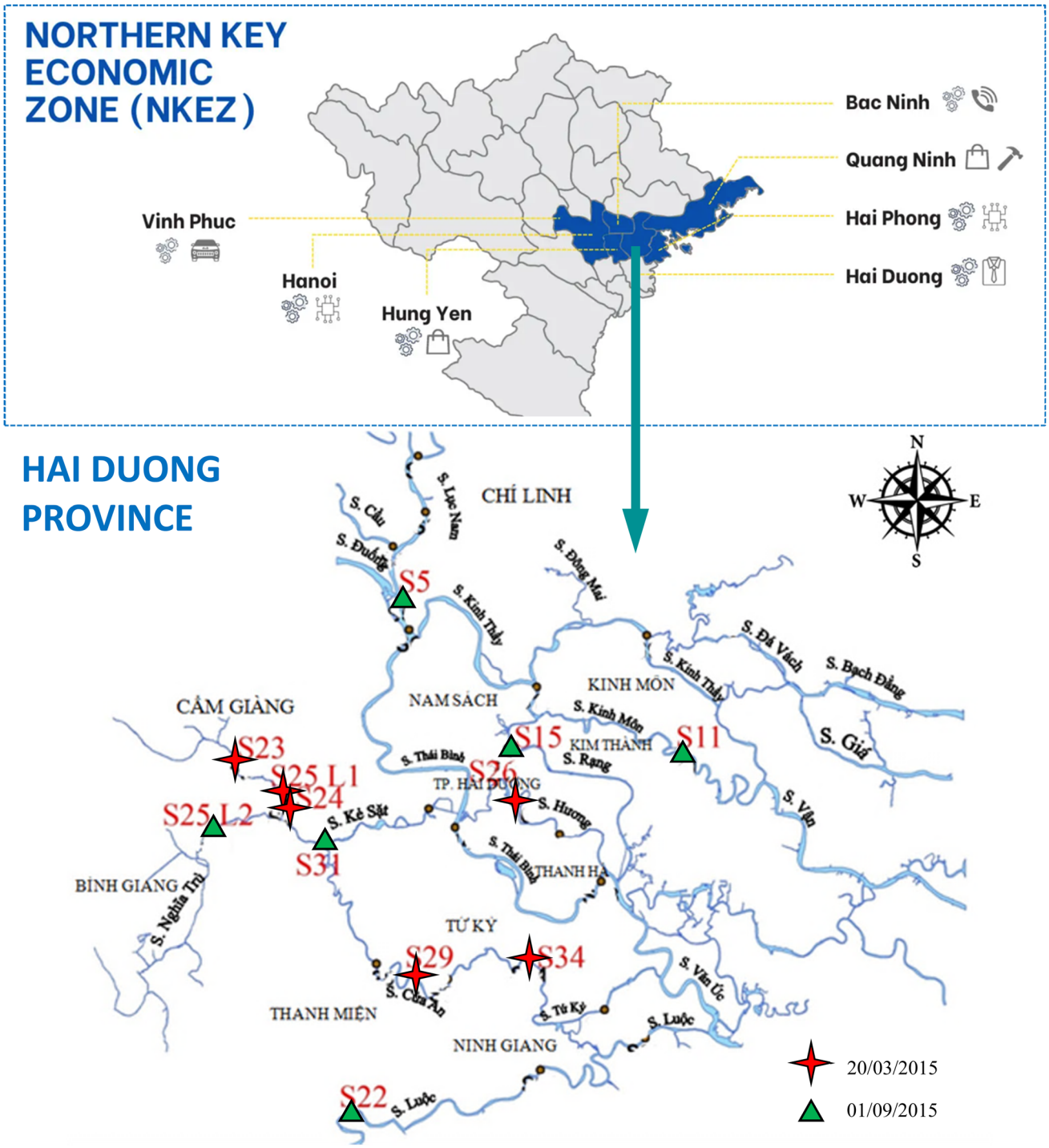


Fig. 1 Map of sampling stations (star: first campaign and triangle: second campaign) in Hai Duong province, Vietnam. The rivers flow in the direction indicated by a northwest to southeast transect (top-left to bottom-right).

studies have examined and demonstrated the pollution of HM species at different depths of sediment cores. In addition, it is essential to systematically assess the quality of sediment by using specific techniques and pollution indices in this area.

In this research, we aim to fill this gap by investigating the geochemical speciation, environmental risk assessment, and the contributions to pollution of HMs (Cu, Pb, Cd, Zn, Fe, Co, Ni, Mn, and Cr) using SEP for HM fractionation and ICP-MS for elemental analysis in sediment cores collected from six study sites in the river systems of Hai Duong province. We present analyses for (1) qualitatively comparing the concentrations of HM species at different sediment depths, (2) rationalizing the distribution pattern of HMs amongst the geochemical phases, (3) quantitatively assessing the sediment quality by estimating the environmental risk of each metal along the sediment depth *via* the contamination factors ($C_f$) and risk assessment code

(RAC), and (4) predicting the apportionment of pollution sources and polluted areas by using multivariate statistical analyses. We illustrate the first-ever demonstration of cross-referencing data from the DNRE to address the long-standing central question of fluxes of HMs in sediments. These results provide a valuable indication for further studies in planning remedy strategies in polluted areas.

## 2. Materials and methods

### 2.1. Study area

The study area of our interest was selected from the river system in Hai Duong province, which is shown in detail in Table 1. The river system in Hai Duong province is located approximately between 20°42′–21°03′N and 106°09′–106°33′E (Fig. 1). Geographically, Hai Duong has a dense network of rivers with two major river systems: the Thai Binh and Bac Hung Hai River systems. Crossing Hai Duong province, the Thai Binh River is roughly 73 km long and receives 30–40 billion $m^3$ of water per year. The Thai Binh River has three tributaries (the Luc Nam, Cau, and Duong rivers) and is of pivotal importance for mineral, cement, and building materials transportation. However, the Bac Hung Hai River, which was built in 1958, is 200 km long, including the Sat, Cam Giang, Thau, Do Day, Dinh Dao, Tu Ky, and Cau Xe rivers, as well as the canal and dike systems that serve as agricultural irrigation for the major cities in Bac Ninh, Hung Yen, and Hai Duong provinces. Therefore, these rivers have been subject to industrial release and agricultural and domestic sewage from Hai Duong province, which have made a discernible contribution to the deterioration of water and sediments.

The authors opted for the sampling sites according to the reference data of the Center of Environmental Monitoring and Analysis, Vietnamese Department of Natural Resources and Environment (DNRE) – Hai Duong province about polluted areas and industrial zones from 2009 to 2014.[52] Samples were collected from the twelve studied sites in the northern part of the Hai Duong province during two batches. The first batch of samples, including only pore water samples, was collected at S23, S24, S25L1, S26, S29, and S34 sites (star symbols) during the spring time (20th March 2015), while the second batch of samples, including pore water and sediment core samples were collected during the autumn time (September 1st, 2015) at S5, S11, S15, S22, S25L2 and S31 sites (triangle symbols).

### 2.2. Sample collection and sample pre-preparation

The field technique for collecting pore water samples is dialysis. The sampling device is called a "peeper", which is based on the single-sided design of Hesslein[55] and made of poly(methyl methacrylate) (PMMA), indicated in Fig. S1.† The dimensions of the peeper are 66 cm × 16.5 cm × 2.5 cm. The peeper sampler uses a 0.2 μm polyethersulfone (PES) exchange membrane to cover the perforated stackers (vials). After three weeks, equilibrium conditions were reached, and the peepers were harvested from sampling locations and cleaned with deionised water. A pore water sample was collected by inserting a clean tip and plastic pipet through the PES membrane from three consecutive stackers of 3 cm length on the peeper. Samples were pre-acidified with 65% $HNO_3$ solution to pH ≤ 2, stored in an ice box, and brought to the laboratory for analysis of total HM content.

Sediment cores were collected at six sampling locations in the second campaign on September 1st, 2015, using a locally fabricated core sampler or sediment corer equipped with 40 cm long steel tubes with a diameter of 8 cm (see Fig. S2†). The device was placed perpendicular to the sediment surface on sites and compressed to about 40 cm so that the sediment occupied all of the device's space. The retrieved core was cut into four sections with 10 cm for each. Raw sediments destined for sequential extraction were dried in air and ground into fine powder using an agate mortar. A sieve of 63 μm mesh size was utilized to discard the oversize grains; then, samples were packed in polyethylene air-tight bags and stored in a refrigerator at 2 °C.

### 2.3. Sequential extraction of heavy metals in sediment

All reagents were of analytical reagent grade (certified purity > 99.9%) unless otherwise stated. Double deionized water (Milli-Q Millipore water with a resistivity of 18.2 MΩ cm) was used for all dilutions. Acetic acid $CH_3COOH$ (glacial, 100% Fisher Scientific), hydroxyl-ammonium chloride $NH_2OH{\cdot}HCl$ (ACROS

Table 1 Sampling site description

| Sampling site no. | Sampling site | Geographic coordinates | Description (from the bank: from the bridge) |
|---|---|---|---|
| S23 | Cam Giang bridge | N: 20°58′3.96″ E: 106°10′4.34″ | (8 m: 30 m) |
| S24 | Ghe bridge, Cam Giang | N: 20°56′14.88″ E: 106°12′39.26″ | (5 m: 30 m) |
| S25L1 | Cay bridge, Binh Giang | N: 20°54″16.08″ E: 106°13′53.20″ | (6 m: 60 m) |
| S26 | Cat bridge, Hai Duong | N: 20°55′50.98″ E: 106°19′41.75″ | 20 m from the bank |
| S29 | Neo bridge, Thanh Mien | N: 20°46′55.61″ E: 106°14′35.79″ | (7 m: 70 m) |
| S34 | Van bridge, Tu Ky | N: 20°48′57.02″ E: 106°24′6.98″ | (7 m: 60 m) |
| S5 | Pha Lai bridge, Chi Linh | N: 21°6′10.53″ E: 106°17′51.84″ | Near the Pha Lai thermal power company |
| S11 | Phu Thai, Kim Thanh | N: 20°57′48.70″ E: 106°31′51.77″ | 500 m from the Van River |
| S15 | CCN Lai Vu, Nam Sach | N: 20°59′38.24″ E: 106°24′37.19″ | Near the Lai Vu industrial zone |
| S22 | Tien Phong, Thanh Mien | N: 20°42′1.12″ E: 106°15′9.65″ | Ship berthing sites |
| S25L2 | Ke Sat bridge, Ke Sat | N: 20°54′54.25″ E: 106° 8′57.66″ | 5 m from the bank |
| S31 | Hiep bridge, Ninh Giang | N: 20°45′50.36″ E: 106°17′13.91″ | 70 m from the bridge |

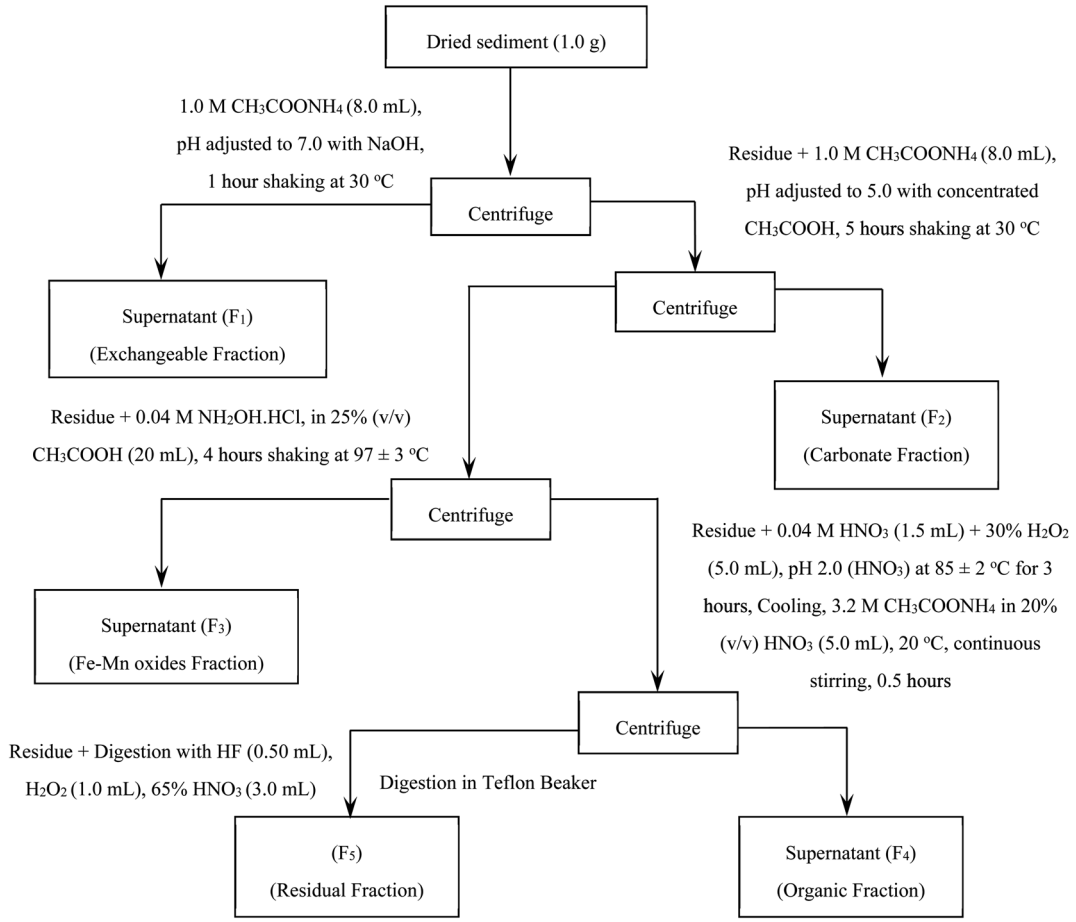


Fig. 2 Schematic representation of the sequential extraction procedure for sediments.

Organics), hydrogen peroxide $H_2O_2$ (30% Fisher Scientific), and ammonium acetate $CH_3COONH_4$ and nitric acid $HNO_3$ (65%, Suprapur Merck, Germany) were of super pure quality (99.950–99.9959%). To mitigate ambiguity in terminology, "element(s)" will henceforth be used interchangeably to denote potentially toxic "HM(s)", unless explicitly defined otherwise.

In order to determine the amounts and geochemical phases of the HMs (Cu, Pb, Cd, Zn, Fe, Co, Ni, Mn, and Cr), a modified five-step sequential extraction procedure (SEP) was adopted.[35] The SEP performance is represented in Fig. 2. Prior to the SEP, the samples were air-dried, ground, and purged with nitrogen (99.999% purity). After each extraction step, the separation of extract from the solid residue was proceeded by centrifugation at 4000 revolutions per minute (rpm) for 25 minutes. The collected fractions were subjected to trace element analysis.

### 2.4. Elemental analysis of heavy metals and method validation

After the SEP, all extracted solutions were kept in polyethylene (PE) containers and stored in a freezer until direct concentration measurements. The determination of HM (Cu, Pb, Cd, Zn, Fe, Co, Ni, Mn, and Cr) concentrations was performed using an ELAN 9000 ICP-MS system (PerkinElmer Sciex, Penlivia, Canada) at the Faculty of Chemistry, VNU University of Science, Hanoi, Vietnam. To mitigate isobaric interference, we carefully chose the isotopes of the investigated elements ($^{53}$Cr, $^{55}$Mn, $^{57}$Fe, $^{59}$Co, $^{60}$Ni, $^{63}$Cu, $^{66}$Zn, $^{111}$Cd, and $^{208}$Pb) to minimize the mass overlapping phenomena. Analytical standard solutions were prepared using nitric acid ($HNO_3$) as a medium, which exerted minimal impact on mass interference with the elements under investigation. Therefore, nitric acid was selected as the matrix for sample solutions in ICP-MS measurements for this study. Nevertheless, our choice of sample matrix and element isotopes did not completely resolve and overcome the mass interference phenomenon for Cd and Pb. Mathematical correction equations for these two HM elements were applied (Table 2).[53]

All glassware (Pyrex) and containers were soaked evenly in 2.00% $HNO_3$ for 24 hours and then rinsed prior to use. Standard metal solutions ($10^3$ mg $L^{-1}$) were either purchased from Merck or prepared in the laboratory from pure metals to establish the calibration curve and determine the detection limit (LOD) and quantitation limit (LOQ) in the ICP-MS method validation procedure. The instrumental LOD and LOQ were evaluated as 3 and 10 times the standard deviation of blank solutions/the intercept divided by the slope of the calibration curve, respectively. To evaluate the LOQ in μg $g^{-1}$ (method LOQ), it is calculated by dividing the instrumental LOQ by the sample

 

Table 2 Operating conditions of ICP-MS and mathematic correction equations for elemental analysis

| Parameters | Conditions |
|---|---|
| ICP-MS system | Elan 9000 (PerkinElmer) |
| Optimized RF power | 1200 W |
| Optimized lens voltage | 8.00 V |
| Optimized nebulizer gas flow rate | 1.05 L $min^{-1}$ |
| Ar plasma gas flow | 15.0 L $min^{-1}$ |
| Auxiliary gas flow | 2.00 L $min^{-1}$ |
| Injection rate | 26 cycles per min |
| Rinsing rate | 48 cycles per min |
| Stabilization rate | 0.10 cycles per s |
| Rinsing time | 120 s |
| Stabilization time | 30 s |
| Rejection parameter $q$ (RPq) | 0.45 |
| Sampling depth | 5.10 mm |
| Replicates per sample | 3 |
| Integration time | 5.80 s |
| Working vacuum pressure | 1.2–1.3 × $10^{-5}$ Torr |
| Standby vacuum pressure | 2.0–3.0 × $10^{-6}$ Torr |

Isobaric correction equations

| Isotope | Isotope ratio | Interference | Correction equation |
|---|---|---|---|
| $^{111}Cd$ | 12.8 | $^{95}Mo^{16}O^+$; $^{94}Zr^{16}OH^+$; $^{39}K_2{}^{16}O_2H^+$ | $I(^{111}Cd) = I(m/z\ 111) - 1.07 \times [I(^{108}MoO) - 0.712 \times I(^{106}Pd)]$ |
| $^{208}Pb$ | 52.4 | $^{192}Pt^{16}O^+$ | $I(^{208}Pb) = I(m/z\ 208) + 1.00 \times I(^{206}Pb) + 1.00 \times I(^{207}Pb)$ |

mass (g) and then multiplying by the dilution volume (L) used for the decomposition.

The calibration curves for Pb, Mn, Ni, Zn, Co, Cu, Cd, and Cr were constructed with four points at concentrations of 4.00 ppb, 20.0 ppb, 100 ppb, and 200 ppb. The calibration curve for Fe was solely based on concentrations of 8.00 ppb, 40.0 ppb, 200 ppb, and 400 ppb. All calibration curves achieved a standard deviation, resulting in $R > 0.999$. The LODs for nine elements (Cr, Mn, Fe, Ni, Co, Cu, Zn, Cd, and Pb), expressed in parts per trillion (ppt or $10^{-12}$ g $mL^{-1}$), were 1.80, 11.4, 20.1, 16.7, 17.8, 15.0, 11.4, 12.3, and 4.20, respectively. Their method LOQs in $10^{-5}$ μg $g^{-1}$ were 4.50, 28.5, 50.2, 41.8, 44.5, 37.5, 28.5, 30.8, and 10.5, respectively.

To validate the accuracy of our method, we assessed bias by obtaining reference values through two approaches: certified reference material (CRM) and spiking studies. The CRM used in this study was MESS-3, a marine sediment material with certified values from the National Research Council of Canada. Our analyses showed that the relative bias (RB) and relative standard deviation (RSD) values in both approaches were below 15.0%, complying with FDA guidelines or SANTE/SANCO guidelines (<20.0%). When analyzing the MESS-3 reference sample, the maximum RB value was 4.15%, and the maximum of RSD was 7.98%. For the standard addition method, the highest RB was 5.45%, and the highest RSD was 2.56%. Hence, it can be concluded that this analytical method achieved acceptable precision and trueness, meeting the accuracy requirements for simultaneous analyses of HM content in sediment cores.

The concentrations of five geochemical components (exchangeable fraction, carbonate fraction, Fe–Mn oxide fraction, organic fraction, and residual fraction) in the sediment cores determined by ICP-MS were converted to percentage terms of the five selective fractions $F_1$, $F_2$, $F_3$, $F_4$, and $F_5$ using eqn (1).

$$F_i\,(M) = \frac{[M]_{F_i}}{\sum_{i}^{n=5} [M]_{F_i}} \times 100\ (\%) \quad (1)$$

$F_i(M)$ is the percentage of element $M$ in fraction $i$; $[M]_{F_i}$ is the concentration of element $M$ in fraction $i$; $\sum_i^{n=5} [M]_{F_i}$ is the total concentration of element $M$ from five specific fractions. The normalization condition follows eqn (2).

$$\sum_{i}^{n=5} F_i(M) = 100 \quad (2)$$

The fractionation of each metal is indicated in the distribution column profile (Sections 3.1 and 3.2) at different sampling sites at different depths of sediments.

### 2.5. Environmental risk assessment of heavy metals

In order to estimate the level of HM pollution in sediment quantitatively, the contamination factors ($C_f$) of elements and risk assessment code (RAC) in the sediment core samples are required.

**2.5.1. Contamination factor ($C_f$).** The determination of the heavy-metal contamination factor is an essential component that assesses the level of environmental risk of HMs concerning their retention time. A higher contamination factor of HMs corresponds to a lower retention time and a higher risk to the surrounding environment. The individual contamination factor (ICF) of HMs was assumed to be equal to the sum of HM concentrations in the mobile phase (non-residual phases) divided by the residual phase content (eqn (3)).[56,57] The global contamination factor (GCF) was theoretically calculated as the sum of the individual factors (eqn (4)). The results of ICFs and GCF in sediment samples are summarized in Section 3.3.1, illustrating the estimated contamination factors of each metal in the sediment core samples at all stations.

$$\mathrm{ICF} = \frac{\sum_{i}^{n=4} [M]_{F_i}}{[M]_{F_5}} = \frac{(F_1 + F_2 + F_3 + F_4)}{F_5} \quad (3)$$

$$\mathrm{GCF} = \sum \mathrm{ICF} \quad (4)$$

It is well established in the literature that the retention time for trace metals in sediments is measured as a time span needed to reduce the element concentration by half.[58] ICF values can be used as a relative measure of metal retention in sediments. The lower the ICF values, the higher the relative metal retention.

**2.5.2. Risk assessment code (RAC).** It can be seen that the degrees of association of a metal with different speciation

compositions in the sediment are at different strengths. Therefore, a risk assessment code (RAC), mobility factor (MF), or bioavailability index (BI) is computed to assess the reactivity of sediment and the risk levels towards aquatic life in the presence of HMs.

Bioavailability is a measure of the degree and rate of absorption of a substance by living systems and is the primary measure of toxicity.[59] An increase in adsorptive or "environmentally available" fractions, exchangeable and/or carbonate-bound fractions, which display a dynamic equilibrium between the aqueous phase and sediment of weakly bonded metals, could increase the bioavailable components.[57,60] Since the acid-soluble fractions ($F_1$ and $F_2$) are directly proportional to bioaccessibility, the risk assessment code is defined as the sum of $F_1$ and $F_2$ fractions on the scale of percentage (eqn (5)). Thus, RAC (%) is a crucial factor for estimating the effect of anthropogenic activities such as agricultural runoff and tourism on the environment. The high RAC values have been interpreted as evidence of relatively high lability and biological availability of HMs in sediment.

$$\mathrm{RAC} = \left( \frac{[M]_{F_1} + [M]_{F_2}}{\sum_{i}^{n=5} [M]_{F_i}} \right) \times 100 = F_1 + F_2(\%) \quad (5)$$

**2.5.3. Partitioning of heavy metals between pore water and sediment.** To assess and elucidate the fate, distribution, and ecotoxicological risk of HMs in the water-sediment relationship, one must consider the distribution coefficient (or pseudo-partition coefficient): $K_d$ (g $L^{-1}$). Pore water-sediment partitioning is expressed as the ratio of HM concentration between the water phase (pore water) and sediment phase (eqn (6)). The HM concentration in sediment is calculated from the total concentration in five sequential extracts.[61,62] It can be stated that the HMs with higher $K_d$ values would have higher movement toward the water phase and greater metal remobilization compared with metals with lower $K_d$.

$$K_d = \frac{[M]_{\text{pore water}}}{[M]_{\text{total sequential extraction steps}}} \left[ \frac{\mu g\ L^{-1}}{\mu g\ g^{-1}} \right] \quad (6)$$

### 2.6. Multivariate statistical analysis

Numerous factors control the sources of HMs, including natural erosion, aqueous degradation, and anthropogenic inputs such as pollutants. Therefore, multivariate statistical analyses were performed to evaluate the dynamics of HMs and clarify the pollution contributions of bioavailable HMs in sediment cores. By applying Minitab 16 statistical software, principal component analysis (PCA) and cluster analysis (CA) were conducted. The other calculations were carried out using OriginPro 2018.

**2.6.1. Principal component analysis (PCA).** PCA is a multivariate analysis technique used to reduce the sheer volume of data by eliminating the variables associated with noise and to explore correlations among the investigated variables. Newly formed "latent" variables are called principal components (PCs). Statistically, PCs are orthogonal basis vectors (eigenvectors) of complex data sets where $PC_1$ is in the direction of maximum variation, $PC_2$ possesses the next greatest variation, and so on.[63] In this study, PCA helps transform the data set from nine dimensions in space (corresponding to the concentrations of nine HMs at six sampling sites) into a lower dimensional representation (usually two or three dimensions). The major conditions to define which PCs to include are that the eigenvalues of these components are larger than 1.00, and the total cumulative variance is over 70.0%.

**2.6.2. Cluster analysis (CA).** CA was implemented to categorize the data set into natural groupings of HMs based on the similarities of HMs in bioavailable fractions. Hierarchical agglomerative clustering (HCA) with a bottom-up algorithm, described in a tree-like pattern (dendrogram), was adopted for the grouping performance in the sense that groups contain mutually exclusive sub-groups.[64] HCA utilizes Euclidean distances as a measure of similarity. Ward's minimum variance method was selected since this method minimizes the total intracluster variance, possesses a small space-distorting effect, and is sensitive to outliers. Ward's method has been proven to offer higher accuracy in terms of grouping performance than other clustering mechanisms.[65]

## 3. Results and discussion

### 3.1. Fractionation of heavy metals in sediment cores

The fractionation of HMs between the sediment phases is shown in Fig. 3. The speciation results express a high Cd, Mn, Co, and Ni content in the exchangeable fraction (phase $F_1$), which theoretically harms aquatic biota. In contrast, the exchangeable fractions of Cr and Fe are trivial (<2.00% of the total). Specifically, Cd mostly underscores high concentrations in all samples at all examined sites, whereas the high proportion of Mn concentrations is only recognized at S11, S15, and S31. The percentage of HMs in sediment in the exchangeable phase descends in the following order: Cd, Mn $\gg$ Ni, Co > Zn > Cu, Pb > Fe, Cr. The descending order of binding ability with the carbonate phase (phase $F_2$) is generally Cd > Co > Mn > Ni > Zn > Pb > Cu, Fe, Cr. From the range of percentages of HMs in the carbonate phase, Co (26.3–58.0%), Mn (16.8–66.3%), Ni (16.0–53.1%), Zn (4.42–45.8%), and Pb (6.75–69.7%) represent the majority portion in the carbonate phase, as these metals possess a particularly high affinity towards carbonate $CO_3^{2-}$ and are prone to co-precipitation with carbonate minerals such as calcite $CaCO_3$ and dolomite $MgCO_3 \cdot CaCO_3$. Carbonate-bound Mn exhibits the second-highest abundance among the non-lithogenic fractions. A higher content of Mn in carbonate-bound forms is most likely since Mn with a similar ionic radius to Ca facilitates Ca substitution in the carbonate phase.[62] The lower percentage of Cr (approximately less than 10.0%) associated with the carbonate fraction in the sediment cores is ascribed to the inability of $Cr^{3+}$ to precipitate or complex with carbonates.[12] Among the non-lithogenic fractions, the Fe–Mn (oxyhydr)oxide reducible phase (phase $F_3$) is the leading fraction of most metals except Cu and Cd. This can be attributed to HMs' adsorption, flocculation, and co-precipitation with the colloids

 

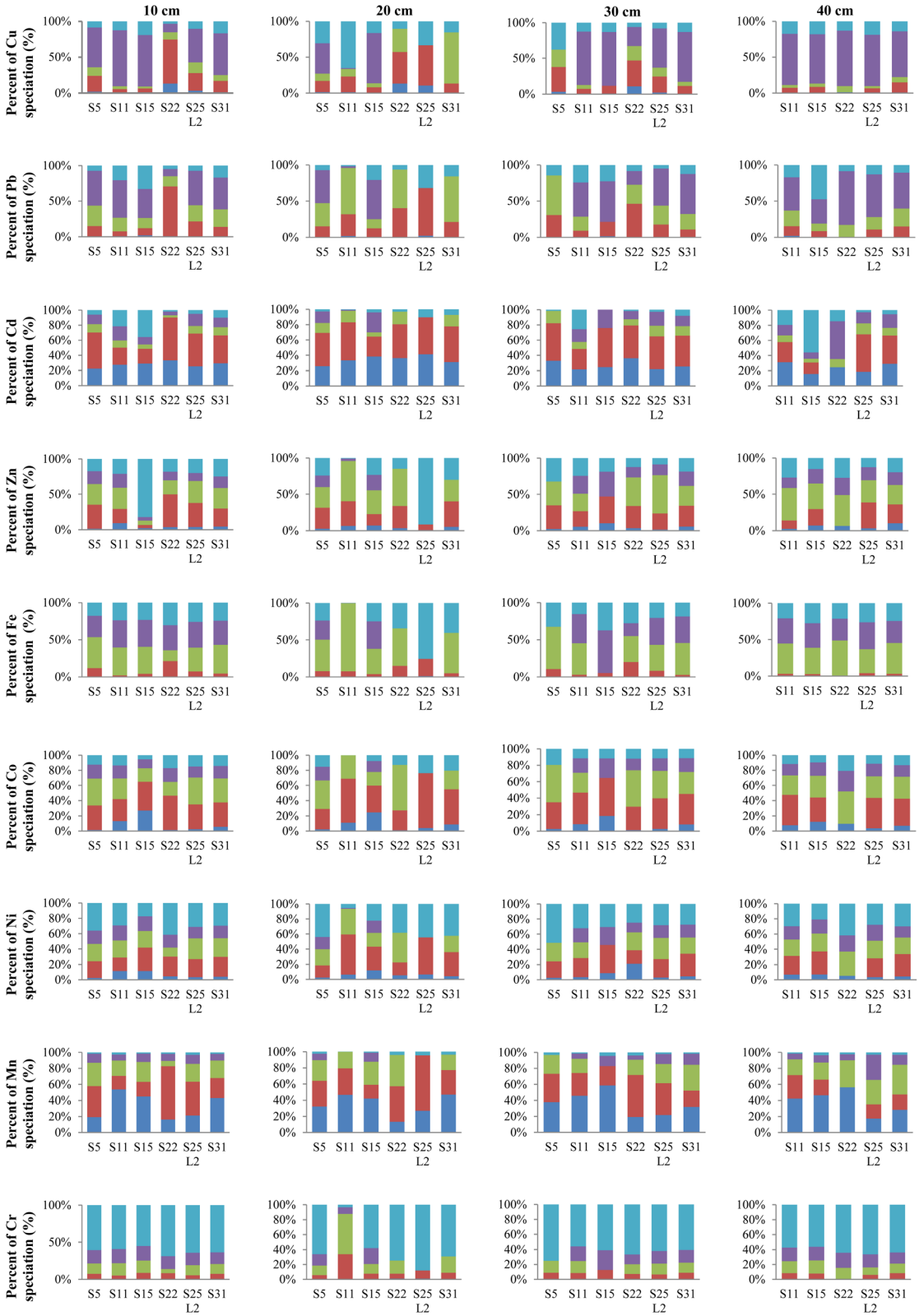


Fig. 3 Metal fractionation of sediment at the six sampling sites (S5, S11, S15, S22, S25L2, and S31) obtained by sequential extractions at depths of 10 cm, 20 cm, 30 cm, and 40 cm (blue: residual, violet: organic, green: Fe–Mn oxide, red: carbonate, and dark blue: exchangeable).

of Fe–Mn (oxyhydr)oxides such as FeOOH and MnOOH.[66] Furthermore, organic matter (phase $F_4$) bound Cu, Pb, Fe, Cr, Co, and Ni seem to be the second most dominant fraction among the non-geogenic portions. A smaller fraction of Mn, Ni, and Zn in the organic species compared to other metals is probably a result of competition between the Fe–Mn-organic complex and hydrous Fe–Mn oxide forms.[24] Results of fractionation analysis suggest that the residual fraction (phase $F_5$) is primarily dominated by Cr (54.9–68.6%), Ni (17.1–43.9%), and Fe (15.5–37.4%) distribution in the sediment core. The metal concentration in the residual fraction pertains to the contribution of natural sources. A higher concentration percentage in this fraction indicates a lower pollution level and the geological derivation of the metals in sediments of the studied region since the residual solid should principally constitute primary and secondary minerals. These minerals may tightly hold those metals within their crystal structure even if they are under the conditions typically encountered in nature over a reasonable time span.[35] Therefore, the high percentages of Cr, Ni, and Fe in the residual fraction demonstrate that they are relatively stable and have weak bioavailability and toxicity.

Overall, the total concentration in the five fractions of HMs from the six sampling sites is similar, highlighting a decrease from the surface of the cores to deeper layers, especially for Cu from 26.9 μg $g^{-1}$ at 10 cm to 4.82 μg $g^{-1}$ at 40 cm at the S22 site. Surface enrichment may arise from the recent enrichment of metals in the water column, which has been interpreted as pollution in recent years. This is because the pollutants are always absorbed into the top sediment first and then sink into the deeper layers by the chemical exchange process.[67] Higher contents of Pb, Cd, Ni, Cu, and Zn in the top layer of sediment at S22, S11, and S15 reveal that these three sites experienced more negative impacts from pollution than the other sites. This pollution can be traced to various anthropogenic activities such as sand exploitation (site S22) or industrial wastewater effluent (Lai Vu industrial zone near S15). The amount of metal species derived from those activities is dominantly in non-residual fractions. The difference becomes smaller at greater depths. This propensity is explained as the HMs in the non-residual fractions are mainly caused by pollution in the top sediments. At greater depths, the trace of recent pollution is less, and the species distribution depends on the geology and hydrology of sediment.

### 3.2. Variation of metal species distribution with depth

Regardless of sampling sites and depths, the phase distribution (based on % metal speciation) of the studied metals in sediment core samples generally followed the orders given below.

Cd: exchangeable ≈ carbonate > residual ≈ organic > Fe–Mn oxide.
Mn: exchangeable ≈ carbonate > Fe–Mn oxide > organic > residual.
Fe: Fe–Mn oxide > organic > residual > carbonate > exchangeable.
Zn: carbonate ≈ Fe–Mn oxide > residual > organic > exchangeable.
Co: carbonate > Fe–Mn oxide > organic ≈ residual > exchangeable.
Cu: organic > residual > carbonate > Fe–Mn oxide > exchangeable.
Pb: organic > carbonate > Fe–Mn oxide > residual > exchangeable.
Ni: residual > carbonate > Fe–Mn oxide > organic > exchangeable.
Cr: residual > organic ≈ Fe–Mn oxide > carbonate > exchangeable.

Based on their similar association with the different phases shown above, the distribution patterns of HM species are divided into four specific groups. The first classification consists of a group bound to labile phases (exchangeable and carbonate) with the presence of Cd and Mn (Section 3.2.1). The second group is associated with Fe–Mn oxides and comprises Co, Zn, and Fe (Section 3.2.2). Cu and Pb (Section 3.2.3) are predominant in the third group associated with organic matter. Lastly, Cr and Ni (Section 3.2.4) are identified to be mainly present in the group bound to residual components.

**3.2.1. Distribution variation of Cd and Mn in the sediment core.** The fractionation profile of Cd with the majority percentage of the labile phase depicts a different pattern than the other metals (exchangeable ≈ carbonate > residual ≈ organic > Fe–Mn oxide). The tendency of various phases of Mn produced a similar order of extraction to Cd: exchangeable ≈ carbonate > Fe–Mn oxide > organic > residual. The remarkable fraction of Cd and Mn in the carbonate form indicates that at a slight lowering pH, a pronounced percentage of Cd would have been remobilized and become readily bioavailable.[68] The favourable co-precipitation of $CdCO_3$ (p$K_{sp}$ 11.7) and $MnCO_3$ (p$K_{sp}$ 10.4) and their subsequent incorporation into the calcite lattice (p$K_{sp}$ 8.42) to form $Ca_{1-x}Cd_xCO_3$ and $Ca_{1-y}Mn_yCO_3$ ($0 \leq x, y \leq 1$) result from the similarity of the ionic radii of Ca (0.99 Å), Cd (0.97 Å), and Mn (0.97 Å) ($K_{sp}$ is the solubility product constant and $pK_{sp} = -\log(K_{sp})$).[69,70] Additionally, the $Ca^{2+}$–$Cd^{2+}$ ion exchange equation $Cd^{2+}(aq) + CaCO_3(s) \rightleftarrows Ca^{2+}(aq) + CdCO_3(s)$ with $K_e \approx 1.00$ at low pH suggests that $Ca^{2+}$ and $Cd^{2+}$ have nearly equal affinity for clay exchange sites ($K_e$ is the equilibrium constant).[71] Thus, the ready access of $Cd^{2+}$ into the $CaCO_3$ structure allows surface precipitation. The high percentage of Cd and Mn in the labile phase (exchangeable, carbonate, *etc.*) reveals that Cd and Mn are the most mobile elements. Since Cd is an accumulative poison for mammals, its main pathways to enter the natural environment are waste products from Cd–Ni batteries, welding, metal refining, electroplating, and pesticide fertilizer.[72] Otherwise, Mn and Fe are probably rooted in natural availability because they are classified into siderophile (iron-loving) elements according to the Goldschmidt geochemical classification. It is recognized that in most natural waters, $Mn^{2+}$ oxidation is a much slower process than $Fe^{2+}$ oxidation. In this phase, weakly adsorbed Mn retained on the sediment surface by relatively weak electrostatic interactions may be released by the cation exchange processes and spontaneous dissociation of $MnCO_3$, MnOOH, and $Na_4Mn_{14}O_{27}\cdot 9H_2O$ minerals. This result refers to a marked amount of Mn that may be liberated into the circumambient environment

 

if conditions are more acidic or reducing. The minor role of the organic fraction in the speciation of Cd and Mn is consistent with the low adsorption to organic matter and with evidence that Cd and Mn do not appear to induce the formation of strong metal–organic complexes.[73]

**3.2.2. Distribution variation of Zn, Co, and Fe in the sediment core.** The proportion of Zn in the sediment was generally in the following order: Fe–Mn oxides ≈ carbonate > residual > organic > exchangeable (except at S15 of the 10 cm top sediment, where residual > Fe–Mn oxides > organic > carbonate > exchangeable). Similar results were reported in surface sediments from Malaysia.[74] The highest levels of Zn appear in weakly bound carbonate and reducible fractions ($F_2$ and $F_3$) with an average of 50.0% or above, suggesting that carbonate and Fe/Mn hydrous oxides are the primarily scavengers of Zn in the river, especially the Zn bound to Fe–Mn oxide fraction which shows a substantive relationship with reducible Mn and reducible Fe concentrations.[75] A major part of Zn is associated with the Fe–Mn oxide phase because of the high stability constants of Zn oxides. Iron oxides adsorb considerable quantities of Zn, and these oxides may also occlude Zn in the lattice structures.[71] On the other hand, Co in each fraction entirely followed the order: carbonate > Fe–Mn oxide > organic ≈ residual > exchangeable. At all sites at different depths, Co was generally distributed among the carbonate (38.0%), reducible (32.0%), and residual fractions (13.0%) on average. Hence, Co was bound to the Fe–Mn oxide fraction at all depths at all sites, which can be explained by the preferential association of Co with Fe and Mn oxides and hydroxides *via* chemisorption and co-precipitation phenomena from industrial pollution in this area. The complexes of $Co^{2+}$ and organic matter are fairly labile so that organically bound $Co^{2+}$ is bioavailable.[71,76] As mentioned above, Fe is categorized as a siderophile element, so it is reasonable that Fe-(hydr)oxides serve as the main reservoir of this element *via* adsorption or co-precipitation. The minor proportion of the labile phase ($F_1$ and $F_2$) in the speciation pattern of Fe shows its preference for being retained and assembled in the sediment structure.

**3.2.3. Distribution variation of Cu and Pb in the sediment core.** In six sampling stations, the distribution profile of Cu and Pb indicates that the substantial portions (close to 70.0% except in the cases of Cu at 20 cm in S11 and Pb at 40 cm in S15) are retained in the non-residual fractions. Cu and Pb can be retained by sediment through exchange and specific adsorption, but precipitation may also be an essential mechanism of retention in polluted sediments.[77] For Cu and Pb, organic matter inputs from nearby aquacultural facilities and anthropogenic discharges from Hai Duong city are the primary "cation carriers" facilitating $Cu^{2+}$ and $Pb^{2+}$ diffusion in the sediment cores. The adsorption of Cu is generally more significant than that of other metals; however, the effective binding of $Cu^{2+}$ and $Pb^{2+}$ ions to soluble organic chelating ligands, driven by favorable enthalpy (strong bonding) and entropy (disorder of sediment-bound entities), may significantly enhance their mobility in sediments.[78] Both Cu and Pb have a higher affinity for particulate organic matter to form stable complexes with high stability constants ($\beta \gg 10^6$) of $Cu^{2+}$/$Pb^{2+}$–organic complexes due to two factors. Firstly, $Cu^{2+}$ and $Pb^{2+}$ are strongly chalcophilic (sulfide ore-loving or chalcogen-loving) and relatively large, polarizable ions with low charge density (borderline acids) favoring bonding to "softer" selective organic sulfur-containing ligands (the principles of Pearson or Hard-Soft Acids and Bases (HSAB) theory).[79] Secondly, $Cu^{2+}$ and $Pb^{2+}$ complex moderately well with organonitrogen moieties (amine and amide) or polyphenols (phenolic –OH groups) in humus by chelate effect, due to good d-orbital overlap.[80] The non-residual fractions depict a normal reducing trend with increasing the depth of sediment cores. Most Cu in the two middle layers (20 cm and 30 cm) is noted in the organic, carbonate, and Fe–Mn oxide fractions at all sites, except in S11 at 20 cm. Cu appears mainly in carbonate up to 20.0% on average, iron and manganese oxides (10.0%), and the residual fraction (20.0%, except in the deepest layer at all sites). On the other hand, the dramatic presence of Pb in the Fe–Mn oxide fraction indicates that Fe–Mn oxides are involved in trapping Pb in both natural and polluted sediment, particularly under basic medium (pH > 7) because of the Mn oxidation of $Pb^{2+}$ to $Pb^{4+}$, which is a very insoluble ion. A high percentage of carbonate (>20.0%) denotes the great domination of Pb in the carbonate fraction, which is similar to what Kierczak *et al.* observed in contaminated dump soil.[81] A higher percentage of Pb is determined in the carbonate phase at the two middle layers rather than the top and the deepest layers. Regarding sampling stations, it has been revealed that Pb is more mobile and potentially more bioavailable at S22. Prifti *et al.* and Altundag *et al.* arrived at comparable results for Pb in regions influenced by anthropogenic activities, with trace metals that were mostly detected in the labile fraction.[14,82]

**3.2.4. Distribution variation of Cr and Ni in the sediment core.** Most of the Cr and Ni are held in all fractions at all sites, except in the middle layer (20 cm) at site S11 (Fig. 3). The dominant phase is in the residual fraction, which accounts for more than 60.0% of Cr and 30.0% of Ni on average in our study and was also found by Kierczak *et al.*[81] and Davutluoglu *et al.*[83] An influential association of Cr and Ni with the residual fraction can be deciphered by the nature of these two metals from the Goldschmidt geochemical classification.[84] Particularly, Cr, a lithophile (rock-loving), and Ni, a siderophile (iron-loving), primarily link to more resistant mineralogical phases, such as crystalline iron oxide and residual silicate phases. Minerals in the residual fraction are strongly bound to metals and do not represent an environmental risk. A smaller portion of Cr in the carbonate phase in relation to the residual can be attributed to the natural properties of the element, such as ionic radius ($r$). Both $Cr^{3+}$ ($r = 61.5$ pm) and $Cr^{6+}$ ($r = 44.0$ pm) ions apparently do not associate with $CO_3^{2-}$ ($r = 178$ pm).[85] A greater percentage of Ni (roughly 45 to 50%) is detected in the carbonate and Fe–Mn oxide fractions compared to Cr (around 20.0%). This phenomenon probably arises from the fact that the ionic radius of $Ni^{2+}$ ($r = 72.0$ pm) is closer to the ionic radius of $CO_3^{2-}$ than Cr ions, even though $Ni^{2+}$ ions are smaller and can be desorbed more easily. Because of the smallest cation radius in the divalent transition metal series, $Ni^{2+}$ easily fits into octahedral sites, co-precipitating readily into Mn and Fe oxides.[71] Thus, Cr ions

are not adsorbed as effectively as $Ni^{2+}$ to the Fe–Mn oxide structure. As chromate $CrO_4^{2-}$, most or all of the $Cr^{6+}$ is spontaneously reduced to $Cr^{3+}$ under acid conditions and the presence of organic matter, which helps stabilize the chromic form. The chromate, therefore, is detoxified and immobilized.[71] However, the distribution at all sites contains up to 15.0% Cr, as well as Ni, within the sulfidic/organic fraction. The percentage of Cr in the organic fraction almost stays unchanged with respect to depth. This finding can be rationalized by the reduction in organic matter and the high correlation of Cr with total organic carbon (TOC).[86] Generally, the higher proportion occurs in the labile phase, leading to a lower portion in the residual phase due to the higher mobility of metals in water-sediment equilibrium. The mobility of Ni in all sediment samples is greater than that of Cr. Consequently, Ni represents a higher risk to the aqueous environment.

### 3.3. Risk assessment of heavy metals in sediments

**3.3.1. Contamination factor ($C_f$).** The sequential extraction data obtained in this study feature a decreasing order of relative retention as follows: Mn > Cd ≫ Pb > Cu > Co > Zn > Fe > Ni > Cr. According to calculated factors in all samples from different depths (Table 3), Mn, Cd, Pb, and Cu may be removed from these sediments at a faster rate than others, which is in accordance with Nemati *et al.*,[87] whereas Cr and Ni seem to have the lowest ability to be released. The residual concentration of any HM is considered the non-mobile fraction and is an essential part of influencing the mobility nature of the HM. In general, anthropogenic metals are more loosely associated with sediment than those of natural origin. The combined effect of Cd, Mn, Pb, and Cu in high concentrations and with high mobility potential presents an increased risk to the ecological system.

Table 4 The relative decreasing order of GCF values of different sites at four depths

| Depth | Average GCF |
|---|---|
| 10 cm | S22 > S5 > S15 > S25L2 > S31 > S11 |
| 20 cm | S15 > S5 > S22 > S31 > S25L2 |
| 30 cm | S25L2 > S22 > S11 > S31 > S5 > S15 |
| 40 cm | S25L2 > S11 > S31 > S22 > S15 |

The GCF tendency generally decreases with depth, although the GCF values are unusual due to the lack of data from S11 at a depth of 20 cm and S5 at a depth of 40 cm. In general, sediments from S5, S22, and S15 in the shallower layers (10 and 20 cm) have the highest ICF and GCF values, meaning that these sampling sites possess the most potential environmental risk. Nonetheless, the S25L2 and S11 sites present more potential ecological risks in the deeper layers than the S5, S22, and S15 sites. Specifically, the trend of the GCF at different depths is expressed in Table 4. Our results identify sites located near the sewage drainage system of the Pha Lai thermal power company (S5) and Lai Vu (S15) and Phu Thai (S11) industrial zones as having high potential environmental risks related to toxic HMs.

**3.3.2. Risk assessment code (RAC).** RAC was determined for the nine trace metals, and the values were interpreted following the RAC classifications (Table 5).[88,89]

Table 3 Individual (ICF) and global contamination factors (GCF) of heavy metals in six sampling sites at different depths

| | | ICF | | | | | | | | | |
|---|---|---|---|---|---|---|---|---|---|---|---|
| Site | Depth | Cu | Pb | Cd | Zn | Fe | Co | Ni | Mn | Cr | GCF |
| S5 | 10 cm | 10.7 | 13.0 | 16.1 | 4.83 | 4.67 | 7.02 | 1.78 | 54.7 | 0.652 | 113 |
| | 20 cm | 2.26 | 13.0 | 35.7 | 3.13 | 3.22 | 5.52 | 1.28 | 38.6 | 0.509 | 103 |
| | 30 cm | 1.64 | 5.98 | 59.2 | 2.11 | 2.06 | 4.12 | 0.945 | 32.1 | 0.329 | 108 |
| S11 | 10 cm | 6.97 | 3.86 | 3.65 | 3.75 | 3.21 | 6.38 | 2.42 | 35.4 | 0.695 | 66.4 |
| | 30 cm | 7.06 | 3.12 | 2.92 | 3.09 | 5.47 | 7.65 | 2.10 | 83.4 | 0.791 | 116 |
| | 40 cm | 4.75 | 4.89 | 4.13 | 2.71 | 3.81 | 7.73 | 2.38 | 59.3 | 0.749 | 90.5 |
| S15 | 10 cm | 4.23 | 2.04 | 1.79 | 0.221 | 3.32 | 17.4 | 4.82 | 63.0 | 0.817 | 97.7 |
| | 20 cm | 5.12 | 3.85 | 24.2 | 3.31 | 3.03 | 12.0 | 3.49 | 84.5 | 0.720 | 140 |
| | 30 cm | 6.77 | 3.44 | — | 4.36 | 1.67 | 7.56 | 2.26 | 22.2 | 0.638 | 48.9 |
| | 40 cm | 4.56 | 1.10 | 0.792 | 5.62 | 2.61 | 9.40 | 3.81 | 28.1 | 0.781 | 56.8 |
| S22 | 10 cm | 27.8 | 20.4 | 53.7 | 4.53 | 2.30 | 4.88 | 1.42 | 50.1 | 0.457 | 166 |
| | 20 cm | 8.50 | 14.6 | 31.2 | 5.78 | 1.91 | 6.74 | 1.62 | 24.1 | 0.340 | 94.8 |
| | 30 cm | 15.7 | 11.2 | 54.4 | 7.13 | 2.60 | 7.39 | 3.03 | 26.3 | 0.498 | 128 |
| | 40 cm | 6.65 | 10.8 | 5.83 | 2.65 | 3.70 | 3.79 | 1.39 | 41.7 | 0.557 | 77.1 |
| S25L2 | 10 cm | 8.55 | 12.8 | 19.7 | 4.04 | 2.85 | 5.75 | 2.20 | 31.2 | 0.560 | 87.7 |
| | 20 cm | 1.99 | 2.14 | 8.65 | 0.0943 | 0.319 | 3.20 | 1.25 | 21.5 | 0.135 | 39.3 |
| | 30 cm | 11.3 | 19.7 | 34.6 | 10.7 | 3.86 | 7.70 | 2.55 | 48.2 | 0.614 | 139 |
| | 40 cm | 4.30 | 6.70 | 36.3 | 6.87 | 2.79 | 7.92 | 2.61 | 33.1 | 0.505 | 101 |
| S31 | 10 cm | 4.96 | 4.97 | 9.04 | 3.03 | 3.13 | 6.08 | 2.38 | 48.8 | 0.574 | 83.0 |
| | 20 cm | 5.45 | 5.33 | 13.0 | 2.33 | 1.47 | 3.93 | 1.35 | 26.4 | 0.444 | 59.7 |
| | 30 cm | 6.72 | 7.05 | 11.4 | 4.39 | 4.40 | 7.76 | 2.65 | 57.0 | 0.653 | 102 |
| | 40 cm | 6.17 | 8.50 | 18.0 | 4.11 | 3.09 | 6.55 | 2.35 | 31.4 | 0.566 | 80.7 |
| Mean values | 10 cm | 10.5 | 9.51 | 17.3 | 3.40 | 3.25 | 7.92 | 2.50 | 47.2 | 0.626 | 102 |
| | 20 cm | 4.66 | 7.78 | 22.6 | 2.93 | 1.99 | 6.27 | 1.80 | 39.0 | 0.430 | 87.4 |
| | 30 cm | 8.20 | 8.40 | 32.5 | 5.30 | 3.34 | 7.03 | 2.26 | 44.8 | 0.587 | 107 |
| | 40 cm | 5.29 | 6.40 | 13.0 | 4.39 | 3.20 | 7.08 | 2.51 | 38.7 | 0.632 | 81.2 |

Table 5 Risk assessment code (RAC)

| Category | Risk | Percentage of acid-soluble fractions (exchangeable and carbonate) (%) |
|---|---|---|
| 1 | No risk (N) | <1 |
| 2 | Low risk (L) | 1–10 |
| 3 | Medium risk (M) | 11–30 |
| 4 | High risk (H) | 31–50 |
| 5 | Very high risk (V) | >50 |

From the selected samples, there were no elements at the no-risk level (<1.00%). The RAC gave values below 10.0% for Cr and Fe, suggesting the high stability of Cr and Fe in the sediments.

From RAC analysis, the mobility was considerably higher in Cu, Pb, and Zn. This means that Cu, Pb, and Zn (medium-risk category) could be noticeable in the near future. However, Cu and Pb in the top sediments also unveil a very high risk at the S22, S5, S25L2, and S11 sites. In category 4, Co and Ni populate the high-risk group. Co and Ni were bound either in the exchangeable or in the carbonate fraction (11.0–30.0%) in most of the sites, which reflects that Co and Ni can easily enter the food chain and pose detrimental impacts on the ecosystem.

In general, this assessment (Table 6) emphasizes that Cd and Mn posed a very high risk (RAC more than 50.0%) at all sampling sites and depths. Because of the toxicity and availability of Cd, it is considered a highly hazardous metal, whereas Mn and Zn are less toxic and essential elements also. There are several sources of Cd in aquatic systems, including runoff containing phosphate fertilizers from agricultural areas near the river. These phosphate fertilizers, applied to agricultural farms, most probably contain Cd.[90] The presence of Cd could also be a result of road traffic, which has been described as a vital source of Cd emission.[91] Therefore, instant supervision and significant remediation must be performed for Cd mobilization as soon as possible.

These sites are located in industrial zones, such as Phu Thai (S11), and the pollution of this area may be imputed to industrial sewage drainage. However, fishery and sand exploitation chiefly mediate the proportion of HMs in S25L2. S5 and S31 are related to the sites affected by municipal sewage from the crowded residential area of Ninh Giang district (S31) and the coal firing process of the Pha Lai thermal power company.

Overall, the results of this study suggest that the mobility and bioavailability of the nine HMs probably decline in the following order: Mn > Cd ≫ Co > Ni > Zn > Pb ≈ Cu ≫ Cr > Fe.

**3.3.3. Partitioning of heavy metals between pore water and sediment.** The $K_d$ analysis results at different depths as well as sites are summarized in Table 7.

From the values of Table 7, the distribution coefficient $K_d$ values are significant compared with modified reference values[92,93] for Cu, Cd, Ni, and Zn at all depths from 10 to 30 cm sediment. Cu, Zn, and Ni with very high $K_d$ values imply that they are bonded weakly to the sediment layer, support metal outspreading into the aquatic environment, and pose an adverse impact. This movement tendency toward the water phase of Cu, Zn, and Cd is quite similar and reasonable with five-fractioning extraction analysis about the high proportion of Cu, Pb, Cd, and Mn in labile/acid soluble phases (exchangeable and carbonate phases), which are easier to transfer to the water phase. On the other hand, Cr, Fe, and Co have much lower $K_d$ values than the others. They have been partitioned in sediment for a longer time due to a higher affinity with the sediment phase than the water phase. The calculated $K_d$ values and the distribution of HMs in two phases, water and sediment, in this

Table 6 Risk assessment code (RAC, %) of heavy metals in the sediments with different depths

| Site | Depth | Cu | Pb | Cd | Zn | Fe | Co | Ni | Mn | Cr |
|---|---|---|---|---|---|---|---|---|---|---|
| S5 | 10 cm | 23.8 | 15.2 | 70.3 | 35.2 | 11.8 | 33.5 | 24.2 | 57.8 | 7.52 |
| | 20 cm | 17.2 | 15.4 | 69.2 | 31.3 | 7.84 | 29.1 | 18.5 | 64.0 | 5.66 |
| | 30 cm | 37.7 | 30.7 | 82.4 | 34.6 | 10.7 | 35.0 | 24.3 | 73.2 | 8.89 |
| S11 | 10 cm | 5.54 | 7.67 | 50.2 | 29.2 | 2.05 | 42.0 | 29.1 | 70.5 | 5.09 |
| | 20 cm | 22.8 | 31.6 | 83.6 | 40.5 | 7.73 | 69.0 | 59.4 | 79.5 | 33.9 |
| | 30 cm | 7.36 | 9.34 | 48.4 | 26.5 | 2.99 | 46.6 | 28.7 | 74.2 | 8.63 |
| | 40 cm | 7.39 | 15.7 | 57.9 | 14.0 | 3.11 | 47.5 | 31.5 | 71.5 | 8.37 |
| S15 | 10 cm | 6.49 | 12.1 | 48.6 | 6.83 | 4.33 | 64.9 | 41.8 | 63.0 | 8.81 |
| | 20 cm | 8.13 | 12.6 | 64.3 | 22.6 | 3.82 | 59.7 | 43.1 | 59.1 | 7.62 |
| | 30 cm | 11.6 | 21.3 | 75.9 | 47.0 | 5.37 | 64.6 | 45.7 | 83.0 | 12.5 |
| | 40 cm | 8.83 | 8.67 | 30.8 | 29.4 | 2.72 | 44.1 | 37.1 | 65.9 | 7.72 |
| S22 | 10 cm | 74.6 | 70.6 | 90.1 | 49.6 | 21.1 | 46.6 | 30.4 | 82.5 | 8.27 |
| | 20 cm | 57.1 | 40.1 | 80.4 | 33.7 | 15.1 | 27.4 | 22.6 | 57.2 | 7.54 |
| | 30 cm | 46.9 | 46.2 | 79.4 | 33.8 | 20.0 | 29.6 | 38.6 | 71.7 | 7.25 |
| | 40 cm | 1.25 | 0.0400 | 24.6 | 6.74 | 0.0815 | 9.49 | 5.25 | 56.4 | 0.572 |
| S25L2 | 10 cm | 27.7 | 21.3 | 68.9 | 37.4 | 7.45 | 34.9 | 27.0 | 63.2 | 5.50 |
| | 20 cm | 66.6 | 68.2 | 89.6 | 8.62 | 24.2 | 76.2 | 55.6 | 95.6 | 11.9 |
| | 30 cm | 24.3 | 17.7 | 65.0 | 23.4 | 8.41 | 39.7 | 27.2 | 61.4 | 6.51 |
| | 40 cm | 6.63 | 11.0 | 67.9 | 38.7 | 4.05 | 43.6 | 28.4 | 35.3 | 6.05 |
| S31 | 10 cm | 16.9 | 13.9 | 66.5 | 29.7 | 4.57 | 37.6 | 29.9 | 67.9 | 7.51 |
| | 20 cm | 13.3 | 21.1 | 77.6 | 40.1 | 5.07 | 55.0 | 36.2 | 77.4 | 8.91 |
| | 30 cm | 11.4 | 10.9 | 66.0 | 34.1 | 2.84 | 45.1 | 34.5 | 52.1 | 8.91 |
| | 40 cm | 15.0 | 15.3 | 66.5 | 35.9 | 3.06 | 42.3 | 34.0 | 47.3 | 8.22 |
| Average | | 22.5 | 22.5 | 66.3 | 30.0 | 7.76 | 44.5 | 32.8 | 66.5 | 8.77 |

Table 7 Distribution coefficients ($K_d$) of heavy metals between pore water and sediment

| Depth | Site | Cu | Pb | Cd | Zn | Fe | Co | Ni | Mn | Cr |
|---|---|---|---|---|---|---|---|---|---|---|
| 10 cm | S5 | 6.00 | 0.379 | 1.78 | 6.16 | 0.903 | 0.866 | 2.63 | 0.578 | 0.595 |
| | S11 | 10.6 | 1.58 | 4.30 | 20.1 | 0.376 | 0.378 | 2.85 | 0.608 | 0.822 |
| | S15 | 5.55 | 2.03 | 5.90 | 1.03 | 0.117 | 0.162 | 5.99 | 0.984 | 0.745 |
| | S22 | 0.484 | 0.257 | 0.165 | 2.12 | 0.605 | 0.123 | 0.665 | 0.973 | 0.0229 |
| | S25L2 | 1.04 | 0.327 | 0.679 | 0.744 | 0.611 | 0.526 | 0.561 | 2.67 | 0.0189 |
| | S31 | 3.04 | 1.68 | 7.37 | 4.26 | 0.246 | 0.689 | 1.68 | 1.76 | 0.213 |
| | Mean | 4.45 | 1.04 | 3.37 | 5.74 | 0.476 | 0.457 | 2.40 | 1.26 | 0.403 |
| 20 cm | S5 | 5.86 | 0.655 | 1.85 | 9.81 | 1.32 | 1.05 | 2.16 | 0.973 | 0.408 |
| | S11 | 26.9 | 2.44 | 2.16 | 15.1 | 1.22 | 0.668 | 3.74 | 1.24 | 1.83 |
| | S15 | 8.60 | 1.17 | 1.63 | 6.06 | 0.300 | 0.479 | 6.80 | 1.00 | 0.822 |
| | S22 | 0.694 | 0.177 | 0.608 | 1.54 | 0.377 | 0.239 | 1.04 | 2.16 | 0.187 |
| | S25L2 | 7.33 | 1.30 | 0.337 | 0.442 | 1.00 | 0.796 | 1.96 | 3.13 | 0.0878 |
| | S31 | 6.22 | 2.75 | 9.20 | 8.77 | 0.160 | 0.286 | 2.18 | 0.269 | 0.249 |
| | Mean | 9.26 | 1.42 | 2.63 | 6.95 | 0.729 | 0.586 | 2.98 | 1.46 | 0.597 |
| 30 cm | S5 | 18.5 | 0.990 | 2.93 | 13.9 | 3.11 | 1.18 | 3.36 | 2.01 | 0.790 |
| | S11 | 11.5 | 0.717 | 2.01 | 7.38 | 0.922 | 0.733 | 2.18 | 1.10 | 0.389 |
| | S15 | 7.21 | 7.01 | 25.1 | 8.99 | 0.258 | 0.382 | 12.6 | 1.59 | 1.15 |
| | S22 | 0.372 | 0.0425 | 0.152 | 1.23 | 0.0326 | 0.211 | 0.795 | 1.75 | 0.114 |
| | S25L2 | 2.93 | 0.270 | 1.24 | 3.06 | 0.140 | 0.230 | 1.54 | 0.475 | 0.420 |
| | S31 | 3.81 | 0.823 | 2.83 | 3.57 | 0.145 | 0.251 | 1.05 | 0.459 | 0.235 |
| | Mean | 7.39 | 1.64 | 5.71 | 6.36 | 0.767 | 0.498 | 3.59 | 1.23 | 0.515 |
| Reference | | 0.316 | 0.0251 | 0.501 | 0.0794 | — | 0.794 | 0.126 | — | 0.0126 |

study are consistent with the studies of Daoquan Xu *et al.*[62] and Li-Jyur Tsai *et al.*[61] Between different sampling sites, almost all HMs at different depths demonstrate high distribution coefficients $K_d$ at S11, S5, and S15 sites, which are near or even in the drainage and sewage system of Hai Duong industrial zones (Lai Vu and Phu Thai) and Pha Lai thermal power station. Furthermore, some display high values at S31 – Hiep bridge, Ninh Giang, specifically with Cd, Zn, and Co.

Table 8 Comparison of mean HM concentration (μg $g^{-1}$) in sediments of the Cau River basin with other studies and different international sediment quality guidelines (SDGs)

| Location | Cu | Pb | Cd | Zn | Fe | Co | Ni | Mn | Cr | References |
|---|---|---|---|---|---|---|---|---|---|---|
| **Vietnam** | | | | | | | | | | |
| Cau River | 7.63 | 13.5 | 0.140 | 19.6 | 4157 | 2.60 | 3.70 | 272 | 5.05 | This study |
| Bach Dang River | 33.9 | 48.1 | 0.560 | 82.9 | 29 080 | — | 26.5 | 549 | 67.4 | Anh *et al.*[94] |
| Cam River | 82.0 | 92.0 | — | 178 | — | 17.0 | 38.0 | 827 | 90.0 | Ho *et al.*[95] |
| Ha Long Bay | 14.5 | 30.4 | 0.080 | 50.9 | — | — | — | — | — | Dang Hoai *et al.*[96] |
| Ba Lat Estuary | 40.4 | 56.2 | 0.390 | 98.6 | 32 986 | 13.0 | 35.1 | 766 | 75.7 | Anh *et al.*[97] |
| Thai Binh coast | 41.4 | — | 0.260 | 93.1 | — | — | 27.4 | — | 39.6 | Duong *et al.*[98] |
| Van Don-Tra Co coast | 55.3 | 21.8 | 3.90 | 165 | — | 21.7 | 28.5 | — | 134 | Nguyen Nhu *et al.*[99] |
| Mekong River | — | 2.08 | 0.100 | 99.0 | 163 | 4.95 | 8.30 | 172 | — | Nguyen *et al.*[100] |
| **Other countries** | | | | | | | | | | |
| Pearl River, China | 36.0 | 46.8 | — | 137 | — | — | 37.2 | — | 82.3 | Ma *et al.*[101] |
| Payra River, Bangladesh | 34.1 | 14.6 | 0.100 | 66.4 | — | 15.7 | 40.3 | 434 | 44.6 | Sultana *et al.*[15] |
| Gohar Rood River, Iran | 59.5 | 30.0 | 0.100 | 213 | 60 660 | 34.0 | 58.2 | 1802 | 175 | Ashayeri *et al.*[24] |
| Astore River, Pakistan | 13.2 | 22.6 | 0.660 | 36.6 | 25 382 | 24.0 | 23.6 | 16 650 | 24.3 | Ali *et al.*[102] |
| Kunhar River, Pakistan | 14.9 | 12.7 | 2.10 | — | 31 600 | 17.6 | 46.5 | — | 17.4 | Muhammad *et al.*[103] |
| Hooghly River, India | 16.7 | 10.7 | 0.200 | 46.9 | 23 322 | — | 19.8 | 482 | 31.8 | Mondal *et al.*[104] |
| Pazarsuyu Stream, Turkey | 114 | 72.1 | 0.700 | 138 | 42 024 | 20.6 | 23.3 | 1137 | 60.4 | Ustaoğlu *et al.*[105] |
| Nile River, Egypt | 21.5 | 13.9 | 2.70 | 76.4 | 25 500 | 12.1 | 48.6 | 660 | 26.4 | Al-Afify *et al.*[106] |
| **SQGs** | | | | | | | | | | |
| TEL | 18.7 | 30.2 | 0.680 | 124 | — | — | 15.9 | — | 52.3 | MacDonald *et al.*[107] |
| PEL | 108 | 112 | 4.21 | 271 | — | — | 42.8 | — | 160 | MacDonald *et al.*[108] |
| LEL | 16.0 | 31.0 | 0.600 | 120 | 2000 | — | 16.0 | 460 | 26.0 | MacDonald *et al.*[108] |
| SEL | 110 | 250 | 10.0 | 820 | 4000 | — | 75.0 | 1100 | 110 | MacDonald *et al.*[108] |
| ERL | 34.0 | 46.7 | 1.20 | 150 | — | — | 20.9 | — | 81.0 | Long *et al.*[109] |
| ERM | 270 | 218 | 9.60 | 410 | — | — | 51.6 | — | 370 | Long *et al.*[109] |

**3.3.4. Comparison with other studies and sediment quality guidelines.** To validate and understand the pollution status of HMs, the overall mean concentrations of HMs in sediment cores from this study were compared with those found in previous studies conducted in the vicinity of Hai Duong province,[94–98] in different rivers in Vietnam,[99,100] and around the world[15,24,101–106] (Table 8). Moreover, they were also compared with reference values from sediment quality criteria to determine whether they meet the allowed standards. In this study, we applied three standard sets of sediment quality guidelines (SQGs), including: (1) threshold effect level (TEL) and probable effect level (PEL);[107,108] (2) lowest effect level (LEL) and severe effect level (SEL);[108] and (3) effect range low (ERL) and effect range medium (ERM).[109]

Based on the comparison in Table 8, some key points can be surmised: (1) the concentrations of most metals (Cu, Pb, Zn, Fe, Co, Ni, Mn, and Cr) in the Cau River basin are lower than those found in the other locations near Hai Duong province, but manifold higher than the maximum contents of Pb, Fe, and Mn in the Mekong River. Nevertheless, the concentration of Cd is higher than that in Ha Long Bay, the Mekong River, and some international rivers in Bangladesh and Iran. This can be attributed solely to human influence. (2) The values of Cu, Pb, Zn, and Mn in the sediment in the Cau River basin are generally on par with those in the Payra River, Astore River, Kunhar River, and Hooghly River. Meanwhile, Cr, Ni, Fe, and Co have lower concentrations than in other rivers. (3) Almost all HMs are in the lower range of each SQG, especially Cr. This means that the impacts of these metals are moderate and have occasional adverse biological effects on the ecosystem. Nonetheless, Cu still poses a high risk for aquatic organisms. Despite a few differences between each SQG, Cr and Ni are relatively non-labile metals and pose minimal contamination risk to the ecosystem. All in all, Hai Duong province, with its rapid industrialization and urbanization, has experienced pollution caused by anthropogenic activities, similar to that of other developing countries around the world.

### 3.4. Multivariate statistical analysis for source identification of heavy metals in sediments

**3.4.1. Principal component analysis (PCA).** Fig. 4 and Table 9 illustrate loadings of HM variables on the first two PCs and the loading plot on the first three PCs, respectively.

The results indicate that three principal components were extracted from the loadings of nine variables (Cu, Pb, Cd, Zn, Fe, Co, Ni, Mn, and Cr) in sediments of six sampling stations. The concentrations of the nine variables were reduced to three PCs ($PC_1$, $PC_2$, and $PC_3$) whose eigenvalues are greater than 1.00 and cumulative variance is 75.3% (Table 9). Thus, this reduction is statistically significant and sufficient to describe and explain data structure information. The loadings on $PC_1$ and $PC_2$ are depicted in Fig. 4.

Principal component 1 ($PC_1$), corresponding to 35.4% of the total variance, is distinguished by the presence of Cu, Pb, Cd, and Mn with positive loading values (>0.40). In this PC, Cd and Mn make up the largest proportion in the labile fraction (exchangeable and carbonate), whilst organic matter (oxidizable fraction) is presumed to be the major sink of Cu and Pb. In general, one or a combination of non-residual fractions (acid-soluble, organic matter, and Fe–Mn oxide) is the key storage for depositing these metals. Despite the high proportion of Mn in the labile fraction, Mn is still referred to as a lithogenic element.[110] This is due to the fact that Mn is detected in the parent material of sediments. From CF and RAC analyses, it is deduced that these metals are specific contaminant elements from urban runoff, automobile emissions, sewage sludge, and industrial wastewater from Hai Duong's industrial zones in the examined areas. Consequently, these metals are principally supposed to originate from anthropogenic activities, which are in line with the findings of Sundaray *et al.*[12] Based on the above

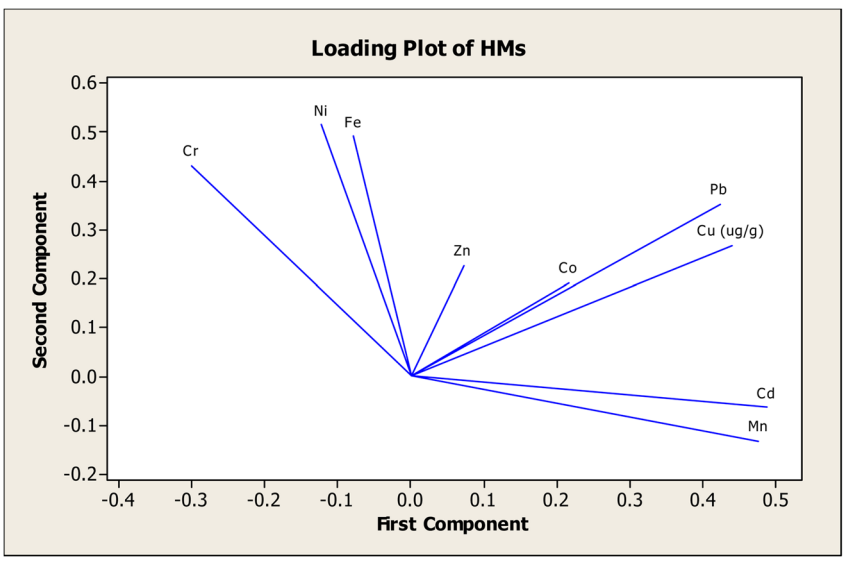


Fig. 4 The loading plot of heavy metals on the first two principal components.

Table 9 The results of principal component analysis for heavy metals in sediments[a]

| | Component | | |
|---|---|---|---|
| Variable | $PC_1$ | $PC_2$ | $PC_3$ |
| Cu | **0.439** | 0.268 | −0.277 |
| Pb | **0.423** | 0.353 | −0.190 |
| Cd | **0.488** | −0.063 | −0.134 |
| Zn | 0.072 | 0.227 | −0.330 |
| Fe | −0.078 | **0.492** | −0.020 |
| Co | 0.217 | 0.192 | **0.734** |
| Ni | −0.123 | **0.515** | 0.355 |
| Mn | **0.476** | −0.133 | 0.261 |
| Cr | −0.301 | **0.431** | −0.165 |
| Eigenvalues | 3.18 | 2.34 | 1.24 |
| Proportion of variance | 0.354 | 0.260 | 0.139 |
| Cumulative proportion | 0.354 | 0.614 | 0.753 |

[a] Bold: these values represent relatively high loadings (absolute values > 0.4) on the components.

reasonings, $PC_1$ may be regarded as the "Anthropogenic Pollutant Source".[111]

Principal component 2 ($PC_2$) covers 26.0% of the total variance and is dominated by Cr, Fe, and Ni with >0.40 loadings. From the fractionation of these metals, the residual phase occupies a prominent ratio amongst the five phases. In contrast with metals in $PC_1$, Cr and Fe exhibit a predisposition to attach longer to the sediment and reveal minor toxicity and less harmful exposure to the environment. The results of CF of Ni are consistent with this proposition, but the RAC and $K_d$ studies otherwise signify Ni as a medium or high-risk element. In addition, Fe is reckoned to be present in the chemical composition of sedimentary rocks in the forms of hematite ($\alpha$-$Fe_2O_3$), goethite ($\alpha$-FeO(OH)), magnetite ($FeO \cdot Fe_2O_3$), limonite ($FeO(OH) \cdot nH_2O$), and siderite ($FeCO_3$).[71] It is inferred that these metals are likely derived from natural parent rock materials, and $PC_2$, therefore, may be ascribed as the "Lithogenic Pollutant Source".[12]

Principal component 3 ($PC_3$) constitutes 13.9% of the total variance and is differentiated by a high positive loading (>0.70) of Co. In the case of Co and Zn, relatively high levels in the carbonate fraction and the Fe–Mn oxide fraction, respectively, are ascertained in all samples. Taking these observations into consideration, $PC_3$ may reflect a combination of source contributions and can be named the "Synergistic Pollutant Source". This component likely emanates from human activities releasing HMs into contiguous environments or the geochemical activities of nature.

**3.4.2. Cluster analysis (CA).** The results of HCA (Fig. 5) reveal two distinct clusters at the 54.8% similarity level: (I) Cu–Pb–Cd–Mn–Co and (II) Cr–Ni–Fe–Zn.

Cluster (I) consists of Cu, Pb, Cd, Mn, and Co, highlighted by the highest percentage bound to the non-residual structure. The contents of these metals are comparable with their corresponding background values, emphasizing that these metals are mainly derived from apparent anthropogenic inputs. However, the metals in the cluster (II) occupy a higher proportion of the residual fraction, especially Cr, implying natural geological sources. Two sub-clusters formed by Co and Zn at a 70.0% similarity level can be individuated. This formation seems to be synonymous with PCA performance.

### 3.5. Summary of results of fractionation, risk assessment, and multivariate analysis

Geochemical speciation data illustrate four defined groups based on the majority proportion in phases: labile-bound group (Cd and Mn), Fe–Mn oxides-bound group (Co, Zn, and

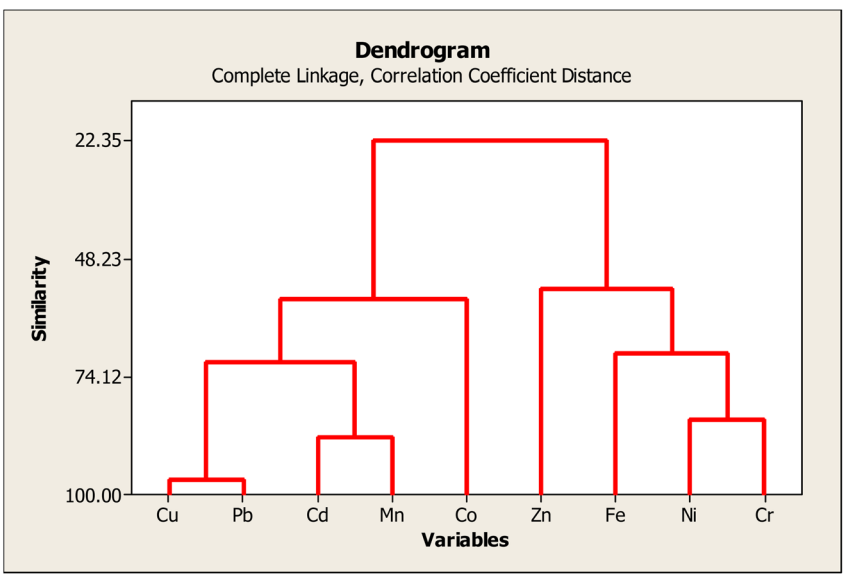


Fig. 5 The dendrogram indicating the similarity of heavy metals.

Fe), organic matter-bound group (Cu and Pb), and residual-bound group (Cr and Ni). First, the qualitative rationales for HMs that dominated in each speciation phase of sediment are taken into account. HMs established in non-residual phases are liable to have weak affinities with sediment, especially the labile-bound group, thus being more mobile. Then, by quantitatively investigating the pollution indices and the transfer of HMs between water and sediment phases *via* the $K_d$ definition, it is obvious to recapitulate that Cd, Mn, Cu, Pb, Zn, and Co may easily manifest severe effects on aquatic ecosystems with headwaters contaminated by industrial zones and manufacturing firms (S5, S11, S15, and S22). Statistically, Cd, Mn, Cu, and Pb are mostly contributed by anthropogenic provenances. Nevertheless, Cr, Ni, and Fe apparently disclose the lower mobility to equilibrate with the water phase and are highlighted by lithogenic sources. The environmental risk assessments of HMs demonstrate harmony with their sediment speciation. These analyses also support our earlier statement that HMs accumulate near the surface of the sediments.

## 4. Conclusions

In this research, a modified five-step SEP and ICP-MS method is presented for geochemical speciation analysis of HM species (Cu, Pb, Cd, Zn, Fe, Co, Ni, Mn, and Cr) in sediment core samples of the Hai Duong river system. The quality of sediment and identification of HM contaminated areas were quantitatively assessed and systematically achieved using environmental risk indices and multivariate statistical analyses. We found that most HMs are dominantly deposited in the top layer of the sediment cores. While Zn and Co showed a high affinity to the carbonate phase and were classified into a "synergistic component", Cr, Ni, and Fe manifested strong adhesion towards primary inert mineral phases and were categorized as the "lithogenic component". In the "anthropogenic component", Mn, Cd, Pb, and Cu may be removed from these sediments at a faster mobility rate than the others and then introduce their widespread potential threat to the neighboring habitat. Our results allocated the contaminated areas of toxic HM pollutants, indicating that they are in close proximity to the sewage drainage system of the Pha Lai thermal power company (S5) and the waste disposal of Lai Vu (S15), Phu Thai (S11) industrial enterprises. Overall, Cd posed a very high risk vulnerability to the surroundings at some polluted stations in the studied area. The remediation and annual monitoring for this metal are recommended. In addition, the adoption of ArcGIS for pollution distribution in density analysis will be further investigated in the next study.

## Data availability

The data used to support the findings of this study have been included in the ESI.†

## Author contributions

Ba Lich Pham: conceptualization, first draft preparation, data treatment, paper writing, editing, and review; Huy Thong Vu and Van Linh Nguyen: chemical analyses and data collection; Thi Kim Thuong Nguyen and Anh Duc Trinh: proofreading and editing; Thi Thao Ta: conceptualization, editing, review, and supervision. All authors have approved the final version of the manuscript for publication and agreed to be held accountable for the work performed therein.

## Conflicts of interest

The authors declare that there are no conflicts of interest regarding this paper.

## Acknowledgements

The authors wish to thank Kenneth Crossley for constructive comments on English grammar and clarity.

## References

1 Ş. Fural, S. Kükrer, İ. Cürebal and D. Aykır, Spatial distribution, environmental risk assessment, and source identification of potentially toxic metals in Atikhisar dam, Turkey, *Environ. Monit. Assess.*, 2021, **193**, 1–16.
2 A. Wali, G. Colinet and M. Ksibi, Speciation of Heavy Metals by Modified BCR Sequential Extraction in Soils Contaminated by Phosphogypsum in Sfax, Tunisia, *Environmental Research, Engineering and Management*, 2014, **4**, 14–26.
3 J.-J. Kim, Y.-S. Kim and V. Kumar, Heavy metal toxicity: an update of chelating therapeutic strategies, *J. Trace Elem. Med. Biol.*, 2019, **54**, 226–231.
4 P. B. Tchounwou, C. G. Yedjou, A. K. Patlolla and D. J. Sutton, Heavy metal toxicity and the environment, *Exper. Suppl.*, 2012, **101**, 133–164.
5 T. Wang, J. Pan and X. Liu, Characterization of heavy metal contamination in the soil and sediment of the Three Gorges Reservoir, China, *J. Environ. Sci. Health, Part A*, 2017, **52**, 201–209.
6 M. A. Okbah, M. I. El-Gammal, M. S. Ibrahim and Y. A. A. Waheshi, Geochemical speciation of trace metals in sediments of the northern Nile Delta Lake by sequential extraction technique, *Chem. Ecol.*, 2020, **36**, 236–255.
7 B. Chen, R. He, P. Cai, G. Huang and F. Wang, Geochemical Speciation, Risk Assessment, and Sources Identification of Heavy Metals in Mangrove Surface Sediments from the Nanliu River Estuary of the Beibu Gulf, China, *Sustainability*, 2022, **14**, 1–20.
8 H. C. Liu and C. F. You, in *Sediment Watch: Monitoring, Ecological Risk Assessment and Environmental Management*, NOVA Science Publishers, 2018, pp. 227–249.
9 M. S. Bhuyan, S. M. B. Haider, G. Meraj, M. A. Bakar, M. T. Islam, M. Kunda, M. A. B. Siddique, M. M. Ali,

S. Mustary, I. A. Mojumder and M. A. Bhat, Assessment of Heavy Metal Contamination in Beach Sediments of Eastern St. Martin's Island, Bangladesh: Implications for Environmental and Human Health Risks, *Water*, 2023, **15**, 2494.

10 S. Bećiragić, J. Huremović, T. Muhić-Šarac, M. Memić, A. Selović and S. Žero, Metal Levels in Surface Soils after Different Extraction Procedures, *Bull. Chem. Technol. Bosnia Herzegovina*, 2013, **41**, 1–5.

11 Y. Qiao, Y. Yang, J. Gu and J. Zhao, Distribution and geochemical speciation of heavy metals in sediments from coastal area suffered rapid urbanization, a case study of Shantou Bay, China, *Mar. Pollut. Bull.*, 2013, **68**, 140–146.

12 S. K. Sundaray, B. B. Nayak, S. Lin and D. Bhatta, Geochemical speciation and risk assessment of heavy metals in the river estuarine sediments - a case study: Mahanadi basin, India, *J. Hazard. Mater.*, 2011, **186**, 1837–1846.

13 T. T. L. Santos, J. L. S. Mounier and R. V. Marins, Trace metal partitioning in the parnaíba delta in dry season, equatorial coast of Brazil, *Environ. Pollut.*, 2024, **345**, 123500.

14 E. Prifti, H. Kaberi, V. Paraskevopoulou, P. Michalopoulos, C. Zeri, S. Iliakis, M. Dassenakis and M. Scoullos, Vertical Distribution and Chemical Fractionation of Heavy Metals in Dated Sediment Cores from the Saronikos Gulf, Greece, *Journal of Marine Science and Engineering*, 2022, **10**, 376–400.

15 S. Sultana, N. Sultana, M. Moniruzzaman, M. R. Dastagir and M. K. Hossain, Unmasking heavy metal contamination: tracing, risk estimating and source fingerprinting from coastal sediments of the Payra River in Bangladesh, *Mar. Pollut. Bull.*, 2025, **211**, 117455.

16 A. Chowdhury, A. Naz and S. K. Maiti, Distribution, speciation, and bioaccumulation of potentially toxic elements in the grey mangroves at Indian Sundarbans, in relation to vessel movements, *Mar. Environ. Res.*, 2023, **189**, 106042.

17 K. K. Jayasooryan, E. V. Ramasamy, P. K. Chandini and M. Mohan, Fractionation and accumulation of selected metals in a tropical estuary, south-west coast of India, *Environ. Monit. Assess.*, 2021, **193**, 220.

18 S. Muhammad, Evaluation of heavy metals in water and sediments, pollution, and risk indices of Naltar Lakes, Pakistan, *Environ. Sci. Pollut. Res.*, 2023, **30**, 28217–28226.

19 S. Muhammad, A. Zeb, M. R. Shaik and M. E. Assal, Spatial distribution of potentially toxic elements pollution and ecotoxicological risk of sediments in the high-altitude lakes ecosystem, *Physics and Chemistry of the Earth, Parts A/B/C*, 2024, **135**, 103655.

20 A. U. Haq, S. Muhammad and A. Ahmad, Spatial Distribution, Risk Assessment, and Provenance of Heavy Metals Contamination in the Sediments of the Gilgit River Basin, Northern Pakistan, *Soil Sediment Contam.*, 2024, **33**, 1365–1381.

21 S. Muhammad and I. Ullah, Spatial and temporal distribution of heavy metals pollution and risk indices in surface sediments of Gomal Zam Dam Basin, Pakistan, *Environ. Monit. Assess.*, 2023, **195**, 1155.

22 A. Mosalem, M. Redwan, A. A. Abdel Moneim and S. Rizk, Distribution, speciation, and assessment of heavy metals in sediments from Wadi Asal, Red Sea, Egypt, *Environ. Monit. Assess.*, 2024, **196**, 215.

23 N. F. Soliman, A. M. Younis and E. Elkady, Chemical speciation and comprehensive risk assessment of metals in sediments from Nabq protectorate, the Red Sea using individual and synergistic indices, *Mar. Pollut. Bull.*, 2024, **201**, 116219.

24 S. Y. Ashayeri, B. Keshavarzi, F. Moore, A. Ahmadi and P. S. Hooda, Risk assessment, geochemical speciation, and source apportionment of heavy metals in sediments of an urban river draining into a coastal wetland, *Mar. Pollut. Bull.*, 2023, **186**, 114389.

25 S. Rezapour, F. Asadzadeh, A. Nouri, H. Khodaverdiloo and M. Heidari, Distribution, source apportionment, and risk analysis of heavy metals in river sediments of the Urmia Lake basin, *Sci. Rep.*, 2022, **12**, 17455.

26 F. Rezaei, M. Rastegari Mehr, A. Shakeri, E. Sacchi, K. Borna and O. Lahijani, Predicting bioavailability of potentially toxic elements (PTEs) in sediment using various machine learning (ML) models: a case study in Mahabad Dam and River-Iran, *J. Environ. Manage.*, 2024, **366**, 121788.

27 Y. Yuan, B. Liu and H. Liu, Spatial distribution and source identification for heavy metals in surface sediments of East Dongting Lake, China, *Sci. Rep.*, 2022, **12**, 7940.

28 Y.-J. Tu, P.-C. Luo, Y.-L. Li, J. Liu, T.-T. Sun, G.-J. Li and Y.-P. Duan, Seasonal heavy metal speciation in sediment and source tracking via Cu isotopic composition in Huangpu River, Shanghai, China, *Ecotoxicol. Environ. Saf.*, 2023, **260**, 115068.

29 W. Sun, K. Yang, R. Li, T. Chen, L. Xia, X. Sun and Z. Wang, Distribution characteristics and ecological risk assessment of heavy metals in sediments of Shahe reservoir, *Sci. Rep.*, 2022, **12**, 16239.

30 Z. Huang, C. Liu, X. Zhao, J. Dong and B. Zheng, Risk assessment of heavy metals in the surface sediment at the drinking water source of the Xiangjiang River in South China, *Environ. Sci. Eur.*, 2020, **32**, 23.

31 W. Que, L. Yi, Y. Wu and Q. Li, Analysis of heavy metals in sediments with different particle sizes and influencing factors in a mining area in Hunan Province, *Sci. Rep.*, 2024, **14**, 20318.

32 Y. Cao, Y. Li, L. Jia, Q. Wang, T. Niu, Q. Yang, Q. Wang, X. Zeng, R. Wang and L. Yue, Long-term and combined heavy-metal contamination forms a unique microbiome and resistome: a case study in a Yellow River tributary sediments, *Environ. Res.*, 2024, **252**, 118861.

33 H. Hu, F. Guo, X. Chen, Y. Wang, J. Liu and H. Cheng, Tin and lead compounds in fish and crustacean from aquaculture ponds in Zhejiang Province of East China: accumulation and health risk assessment, *Aquaculture*, 2025, **595**, 741586.

34 Q. Chen, L. Wu, C. Zhou, G. Liu and L. Yao, A study of environmental pollution and risk of heavy metals in the bottom water and sediment of the Chaohu Lake, China, *Environ. Sci. Pollut. Res.*, 2024, **31**, 19658–19673.
35 A. Hass and P. Fine, Sequential Selective Extraction Procedures for the Study of Heavy Metals in Soils, Sediments, and Waste Materials—A Critical Review, *Crit. Rev. Environ. Sci. Technol.*, 2010, **40**, 365–399.
36 Ś. Ryszard and T. Marzena, Chemical Fractionation in Environmental Studies of Potentially Toxic Particulate-Bound Elements in Urban Air: A Critical Review, *Toxics*, 2022, **10**, 1–29.
37 C. Gleyzes, S. Tellier and M. Astruc, Fractionation studies of trace elements in contaminated soils and sediments: a review of sequential extraction procedures, *TrAC, Trends Anal. Chem.*, 2002, **21**, 451–467.
38 D. J. Butcher, Recent advances in graphite furnace atomic absorption spectrometry: a review of fundamentals and applications, *Appl. Spectrosc. Rev.*, 2024, **59**, 247–275.
39 M. M. López Guerrero, M. T. Siles Cordero, E. Vereda Alonso, A. García de Torres and J. M. Cano Pavón, Cold vapour generation electrothermal atomic absorption spectrometry and solid phase extraction based on a new nanosorbent for sensitive Hg determination in environmental samples (sea water and river water), *Microchem. J.*, 2017, **132**, 274–279.
40 N. Manousi and A. N. Anthemidis, A flow-batch lab-in-syringe foam microextraction platform for the simultaneous preconcentration and in situ membraneless gas-liquid separation of mercury prior to cold vapor atomic absorption spectrometry, *Anal. Chim. Acta*, 2024, **1290**, 342208.
41 M. Patra, S. N. Upadhyay and S. K. Dubey, Synchrotron induced X-ray fluorescence spectroscopy reveals heavy metal translocation in sludge amended soil–plant systems: assessment of ecological and health risks, *Environ. Geochem. Health*, 2024, **46**, 399.
42 E. Marguí, D. Eichert, J. Jablan, F. Bilo, L. E. Depero, A. Pejović-Milić, A. Gross, H. Stosnach, A. Kubala-Kukuś, D. Banaś and L. Borgese, An overview of the applications of total reflection X-ray fluorescence spectrometry in food, cosmetics, and pharmaceutical research, *J. Anal. At. Spectrom.*, 2024, **39**, 1700–1719.
43 Q. Zhang, F. Li and W. Yang, A deep spectral prediction network to quantitatively determine heavy metal elements in soil by X-ray fluorescence, *J. Anal. At. Spectrom.*, 2024, **39**, 478–490.
44 T. T. K. Nguyen, H. T. Luu, L. D. Vu, T. T. Ta and G. T. H. Le, Determination of Total Mercury in Solid Samples by Anodic Stripping Voltammetry, *J. Chem.*, 2021, **2021**, 8888879.
45 S. Laschi, P. S. Sfragano, F. Tadini-Buoninsegni, N. Guigues and I. Palchetti, Development of a flow system for decentralized electrochemical analysis of heavy metals using screen-printed electrodes: the importance of sensor stability, *Analyst*, 2024, **149**, 4239–4249.
46 J. Zhong, Z. Wang, Y. Chen, W. Huan, M. Shi, L. Lei, X. Yu and L. Chen, Determination of trace heavy metal elements in litterfall by inductively coupled plasma optical emission spectrometry after extraction using choline chloride-based deep eutectic solvents, *RSC Adv.*, 2024, **14**, 22497–22503.
47 Erdiwansyah, A. Gani, H. Desvita, Mahidin, Bahagia, R. Mamat and S. M. Rosdi, Investigation of heavy metal concentrations for biocoke by using ICP-OES, *Results Eng.*, 2025, **25**, 103717.
48 C. S. Provete, B. M. Dalfior, R. Mantovaneli, M. T. W. D. Carneiro and G. P. Brandão, Comparison of the Performance of ICP-MS, CV-ICP-OES, and TDA AAS in Determining Mercury in Marine Sediment Samples, *ACS Omega*, 2024, **9**, 49229–49238.
49 F. Guo, P. Zeng, J. Liu, H. Hu, W. Zhu, Y. Wang and H. Cheng, Simultaneous preconcentration and quantification of ultra-trace tin and lead species in seawater by online SPE coupled with HPLC-ICP-MS, *Anal. Chim. Acta*, 2024, **1294**, 342294.
50 M. H. Nguyen, T. D. Pham, T. L. Nguyen, H. A. Vu, T. T. Ta, M. B. Tu, T. H. Y. Nguyen and D. B. Chu, Speciation Analysis of Arsenic Compounds by HPLC-ICP-MS: Application for Human Serum and Urine, *J. Anal. Methods Chem.*, 2018, **2018**, 9462019.
51 T. T. Ta, D. A. Trinh and N. T. Do, Nitrogen flow assessment in rapidly urbanizing Hai Duong province, downstream of Cau River Basin, Vietnam, *J. Mater. Cycles Waste Manage.*, 2018, **20**, 533–542.
52 Hai Duong Department of Natural Resources and Environment, *Report on Water Quality Monitoring during the period 2009–2014 in Hai Duong Province*, Department of Natural Resources and Environment (DNRE), Vietnam, 2014.
53 S. H. Le, A. D. Trinh, H. T. Vu and T. T. Ta, Assessment of surface water quality and nutrient pollution source using multivariate statistical technique: a case study of Cau River Basin in Hai Duong province, *The 4th Analytica Vietnam Conference*, 2015, **25**, 71–79.
54 T. T. Ta, S. H. Le, H. Q. Trinh, T. N. M. Luu and A. D. Trinh, Interpretation of anthropogenic impacts (agriculture and urbanization) on tropical deltaic river network through the spatio-temporal variation of stable (N, O) isotopes of $NO_3^{(-)}$, *Isot. Environ. Health Stud.*, 2016, **52**, 487–497.
55 R. H. Hesslein, An *in situ* sampler for close interval pore water studies, *Limnol. Oceanogr.*, 1976, **21**, 912–914.
56 M. A. M. Abdallah, Chemical speciation and contamination assessment of Pb and V by sequential extraction in surface sediment off Nile Delta, Egypt, *Arabian J. Chem.*, 2017, **10**, 68–75.
57 M. Tytła, Assessment of Heavy Metal Pollution and Potential Ecological Risk in Sewage Sludge from Municipal Wastewater Treatment Plant Located in the Most Industrialized Region in Poland—Case Study, *International Journal of Environmental Research and Public Heath*, 2019, **16**, 24–30.
58 A. Kabata-Pendias, *Trace elements in soils and plants*, Taylor & Francis Group, CRC Press, Boca Raton, 4th edn, 2010.
59 D. Sah, P. K. Verma, M. K. Kandikonda and A. Lakhani, Chemical fractionation, bioavailability, and health risks of

heavy metals in fine particulate matter at a site in the Indo-Gangetic Plain, India, *Environ. Sci. Pollut. Res. Int.*, 2019, **26**, 19749–19762.

60 J. Singh, A. S. Kalamdhad and B.-K. Lee, Reduction of eco-toxicity risk of heavy metals in the rotary drum composting of water hyacinth: waste lime application and mechanisms, *Environ. Eng. Res.*, 2015, **20**, 212–222.

61 L.-J. Tsai, K. C. Yu, J.-S. Huang and S.-T. Ho, Distribution of heavy metals in contaminated river sediment, *J. Environ. Sci. Health, Part A*, 2002, **37**, 1421–1439.

62 D. Xu, Y. Wang, R. Zhang, J. Guo, W. Zhang and K. Yu, Distribution, speciation, environmental risk, and source identification of heavy metals in surface sediments from the karst aquatic environment of the Lijiang River, Southwest China, *Environ. Sci. Pollut. Res.*, 2016, **23**, 9122–9133.

63 J. N. Miller, J. C. Miller and R. D. Miller, *Statistics and Chemometrics for Analytical Chemistry*, Pearson Education Limited, Harlow, United Kingdom, 7th edn, 2018.

64 R. Wehrens, *Chemometrics with R: Multivariate Data Analysis in the Natural and Life Sciences (Use R!)*, Springer, Berlin, Hiedelberg, 2nd edn, 2020.

65 A. S. Luna, *Chemometrics: Methods, Applications and New Research*, Nova, United Kingdom, 2017.

66 C. M. A. Iwegbue, G. E. Nwajei, O. Eguavoen and J. E. Ogala, Chemical fractionation of some heavy metals in soil profiles in vicinity of scrap dumps in Warri, Nigeria, *Chem. Speciation Bioavailability*, 2009, **21**, 99–110.

67 J. Chen, J. Liu, H. Hong, S. Liang, W. Zhao, H. Jia, H. Lu, J. Li and C. Yan, Coastal reclamation mediates heavy metal fractions and ecological risk in saltmarsh sediments of northern Jiangsu Province, China, *Sci. Total Environ.*, 2022, **825**, 1–11.

68 W. Xu, L. Xiao, S. Hou, G. Rukh, M. Xu, Y. Pan, J. Xu, W. Lan, Z. Ruan, B. Zhong and D. Liu, Bioavailability and speciation of cadmium in contaminated paddy soil as alleviated by biochar from co-pyrolysis of peanut shells and maize straw, *Environ. Sci. Eur.*, 2022, **34**, 1–10.

69 S. Cai, S. Zhou, J. Cheng, Q. Wang and Y. Dai, Distribution, Bioavailability and Ecological Risk of Heavy Metals in Surface Sediments from the Wujiang River Basin, Southwest of China, *Pol. J. Environ. Stud.*, 2021, **30**, 5479–5491.

70 T. D. Nguyen and T. P. D. Dao, *Analytical Chemistry, Questions and Problems in Ionic Equilibrium in Aqueous Solutions*, Hanoi National University of Education Publishers, 2005.

71 M. B. McBride and C. E. Martínez, *Environmental chemistry of soils*, Royal Society of Chemistry, New York, 1st edn, 2023.

72 Inamuddin, M. I. Ahamed and E. Lichtfouse, *Water Pollution and Remediation: Heavy Metals*, Springer International Publishing, 2021.

73 H. Ji, H. Li, Y. Zhang, H. Ding, Y. Gao and Y. Xing, Distribution and risk assessment of heavy metals in overlying water, porewater, and sediments of Yongding River in a coal mine brownfield, *J. Soils Sediments*, 2018, **18**, 624–639.

74 A. Naji, A. Ismail and A. R. Ismail, Chemical speciation and contamination assessment of Zn and Cd by sequential extraction in surface sediment of Klang River, Malaysia, *Microchem. J.*, 2010, **95**, 285–292.

75 M. Abidi, A. Yahyaoui, R. B. Amor, L. Chouba and M. Gueddari, Evaluation of heavy metal pollution risk in surface sediment of the South Lagoon of Tunis by a sequential extraction procedure, *Sci. Mar.*, 2022, **86**, 1–12.

76 B. A. Hakami, E.-S. S. A. Seif and A. A. El-Shater, Environmental pollution assessment of Al-Musk Lake, Jeddah, Saudi Arabia, *Nat. Hazards*, 2020, **101**, 429–448.

77 R. B. Amor, A. Yahyaoui, M. Abidi, L. Chouba and M. Gueddari, Bioavailability and Assessment of Metal Contamination in Surface Sediments of Rades-Hamam Lif Coast, around Meliane River (Gulf of Tunis, Tunisia, Mediterranean Sea), *J. Chem.*, 2019, **2019**, 1–11.

78 M. M. Billah, E. Kokushi and S. Uno, Distribution, Geochemical Speciation, and Bioavailable Potencies of Cadmium, Copper, Lead, and Zinc in Sediments from Urban Coastal Environment in Osaka Bay, Japan, *Water, Air, Soil Pollut.*, 2019, **230**, 1–13.

79 R. G. Pearson, Hard and Soft Acids and Bases, *J. Am. Chem. Soc.*, 1963, **85**, 3533–3539.

80 C. E. Housecroft and A. G. Sharpe, *Inorganic Chemistry*, Pearson Prentice Hall, United Kingdom, 5th edn, 2018.

81 J. Kierczak, C. Neel, U. Aleksander-Kwaterczak, E. Helios-Rybicka, H. Bril and J. Puziewicz, Solid speciation and mobility of potentially toxic elements from natural and contaminated soils: a combined approach, *Chemosphere*, 2008, **73**, 776–784.

82 H. Altundag, M. Imamoglu, S. Doganci, E. Baysal, S. Albayrak and M. Tuzen, Determination of Heavy Metals and Their Speciation in Street Dusts by Inductively Coupled Plasma-Optical Emission Spectrometry after a Community Bureau of Reference Sequential Extraction Procedure, *J. AOAC Int.*, 2013, **96**, 864–869.

83 O. I. Davutluoglu, G. Seckin, C. B. Ersu, T. Yilmaz and B. Sari, Heavy metal content and distribution in surface sediments of the Seyhan River, Turkey, *J. Environ. Manage.*, 2011, **92**, 2250–2259.

84 V. M. Goldschmidt, Geochemistry, *Soil Sci.*, 1954, **78**, 156.

85 G. L. Miessler, P. J. Fischer and D. A. Tarr, *Inorganic chemistry*, Pearson, Boston, 5th edn, 2021.

86 A. Wali, G. Colinet, M. Khadhraoui and M. Ksibi, Trace metals in surface soil contamination by release of phosphate industry in the surroundings of Sfax-Tunisia, *Environmental Research, Engineering and Management*, 2013, **65**, 20–25.

87 K. Nemati, N. K. A. Bakar, M. R. Abas and E. Sobhanzadeh, Speciation of heavy metals by modified BCR sequential extraction procedure in different depths of sediments from Sungai Buloh, Selangor, Malaysia, *J. Hazard. Mater.*, 2011, **192**, 402–410.

88 M. N. Islam, X. P. Nguyen, H.-Y. Jung and J.-H. Park, Chemical Speciation and Quantitative Evaluation of Heavy Metal Pollution Hazards in Two Army Shooting Range

 

Backstop Soils, *Bull. Environ. Contam. Toxicol.*, 2016, **96**, 179–185.

89 F. Li, M. Xiao, J. Zhang, C. Liu, Z. Qiu and Y. Cai, Spatial Distribution, Chemical Fraction and Fuzzy Comprehensive Risk Assessment of Heavy Metals in Surface Sediments from the Honghu Lake, China, *Int. J. Environ. Res. Public Health*, 2018, **15**, 1–17.

90 X. Hao, L. Bai, X. Liu, P. Zhu, H. Liu, Y. Xiao, J. Geng, Q. Liu, L. Huang and H. Jiang, Cadmium Speciation Distribution Responses to Soil Properties and Soil Microbes of Plow Layer and Plow Pan Soils in Cadmium-Contaminated Paddy Fields, *Front. Microbiol.*, 2021, **12**, 1–12.

91 L. Gao, R. Li, Z. Liang, L. Hou and J. Chen, Seasonal variations of cadmium (Cd) speciation and mobility in sediments from the Xizhi River basin, South China, based on passive sampling techniques and a thermodynamic chemical equilibrium model, *Water Res.*, 2021, **207**, 1–11.

92 J. D. Allison and T. L. Allison, *Partition coefficients for metals in surface water, soil, and waste*, U.S. Environmental Protection Agency Office of Research and Development, Washington, DC 20460, 2005.

93 J. E. Sedeño-Díaz, E. López-López, E. Mendoza-Martínez, A. J. Rodríguez-Romero and S. S. Morales-García, Distribution Coefficient and Metal Pollution Index in Water and Sediments: Proposal of a New Index for Ecological Risk Assessment of Metals, *Water*, 2020, **12**, 1–20.

94 N. N. Anh, Attribution of sources to heavy metal accumulation in the anthropogenically impacted Bach Dang River Estuary, Vietnam, *Mar. Pollut. Bull.*, 2023, **193**, 115244.

95 H. H. Ho, R. Swennen, V. Cappuyns, E. Vassilieva, G. Neyens, M. Rajabali and T. Van Tran, Assessment on Pollution by Heavy Metals and Arsenic Based on Surficial and Core Sediments in the Cam River Mouth, Haiphong Province, Vietnam, *Soil Sediment Contam.*, 2013, **22**, 415–432.

96 N. Dang Hoai, H. Nguyen Manh, T. Tran Duc, T. Do Cong, L. Tran Dinh, R. Johnstone and D. Nguyen Thi Kim, An assessment of heavy metal contamination in the surface sediments of Ha Long Bay, Vietnam, *Environ. Earth Sci.*, 2020, **79**, 436.

97 N. N. Anh, An insight into source apportionment of metals in superficial sediments from the Tien Hai nature reserve of the Red River delta, Vietnam, *Mar. Pollut. Bull.*, 2022, **185**, 114278.

98 L. T. Duong, B. Q. Nguyen, C. D. Dao, N. N. Dao, H. L. T. Nguyen, T. H. T. Nguyen, C. H. T. Nguyen, D. C. Duong and N. N. Pham, Heavy metals in surface sediments of the intertidal Thai Binh Coast, Gulf of Tonkin, East Sea, Vietnam: distribution, accumulation, and contamination assessment, *Environ. Sci. Pollut. Res.*, 2022, **29**, 41261–41271.

99 T. Nguyen Nhu, N. Bui Van, D.-A. Le, T. H. Tran Thi, T.-D. Nguyen, T. Dang Xuan, H.-N. Tran, P. N. Sang, M. Saiyad Musthafa and V.-H. Duong, Characteristics of heavy metals in surface sediments of the Van Don-Tra Co coast, northeast Vietnam, *Regional Studies in Marine Science*, 2024, **73**, 103459.

100 B. T. Nguyen, D. D. Do, T. X. Nguyen, V. N. Nguyen, D. T. Phuc Nguyen, M. H. Nguyen, H. T. Thi Truong, H. P. Dong, A. H. Le and Q.-V. Bach, Seasonal, spatial variation, and pollution sources of heavy metals in the sediment of the Saigon River, Vietnam, *Environ. Pollut.*, 2020, **256**, 113412.

101 Y. Ma, Y. Ma, W. Zhang, H. Zhang, T. Li, D. Kong, C. Xu, H. Shi, X. Xu and D. Wang, The Spatiotemporal Variation and Historical Evolution of Heavy Metal Pollution in Sediments from the Pearl River Estuary, China, *Water*, 2024, **16**, 531.

102 W. Ali and S. Muhammad, Spatial distribution, eco-environmental risks, and source characterization of heavy metals using compositional data analysis in riverine sediments of a Himalayan River, Northern Pakistan, *J. Soils Sediments*, 2023, **23**, 2244–2257.

103 S. Muhammad, S. Ullah, W. Ali, I. A. K. Jadoon and M. Arif, Spatial distribution of heavy metal and risk indices of water and sediments in the Kunhar River and its tributaries, *Geocarto International*, 2022, **37**, 5985–6003.

104 P. Mondal, M. Schintu, B. Marras, A. Bettoschi, A. Marrucci, S. K. Sarkar, R. Chowdhury, M. P. Jonathan and J. K. Biswas, Geochemical fractionation and risk assessment of trace elements in sediments from tide-dominated Hooghly (Ganges) River Estuary, India, *Chem. Geol.*, 2020, **532**, 119373.

105 F. Ustaoğlu and M. S. Islam, Potential toxic elements in sediment of some rivers at Giresun, Northeast Turkey: a preliminary assessment for ecotoxicological status and health risk, *Ecol. Indic.*, 2020, **113**, 106237.

106 A. D. G. Al-Afify and A. M. Abdel-Satar, Risk assessment of heavy metal pollution in water, sediment and plants in the Nile River in the Cairo region, Egypt, *Oceanol. Hydrobiol. Stud.*, 2020, **49**, 1–12.

107 D. D. Macdonald, R. S. Carr, F. D. Calder, E. R. Long and C. G. Ingersoll, Development and evaluation of sediment quality guidelines for Florida coastal waters, *Ecotoxicology*, 1996, **5**, 253–278.

108 D. D. MacDonald, C. G. Ingersoll and T. A. Berger, Development and Evaluation of Consensus-Based Sediment Quality Guidelines for Freshwater Ecosystems, *Arch. Environ. Contam. Toxicol.*, 2000, **39**, 20–31.

109 E. R. Long, D. D. Macdonald, S. L. Smith and F. D. Calder, Incidence of adverse biological effects within ranges of chemical concentrations in marine and estuarine sediments, *Environ. Manage.*, 1995, **19**, 81–97.

110 J. Madondo, C. Canet, E. González-Partida, A. A. Rodríguez-Díaz, F. Núñez-Useche, P. Alfonso, A. Rajabi, T. Pi, L. Blignaut and N. Vafeas, Geochemical constraints on the genesis of the 'Montaña de Manganeso' vein-type Mn deposit, Mexican Plateau, *Ore Geol. Rev.*, 2020, **125**, 1–16.

111 J. P. Vareda, A. J. M. Valente and L. Durães, Assessment of heavy metal pollution from anthropogenic activities and remediation strategies: a review, *J. Environ. Manage.*, 2019, **246**, 101–118.